Accepted Manuscript

Organoseleno cytostatic derivatives: Autophagic cell death with AMPK and JNK activation

Pablo Garnica, Ignacio Encío, Daniel Plano, Juan A. Palop, Carmen Sanmartín

PII: S0223-5234(19)30402-7

DOI: https://doi.org/10.1016/j.ejmech.2019.04.074

Reference: EJMECH 11309

To appear in: *European Journal of Medicinal Chemistry*

Received Date: 18 February 2019

Revised Date: 17 April 2019

Accepted Date: 29 April 2019

Please cite this article as: P. Garnica, I. Encío, D. Plano, J.A. Palop, C. Sanmartín, Organoseleno cytostatic derivatives: Autophagic cell death with AMPK and JNK activation, *European Journal of Medicinal Chemistry* (2019), doi: https://doi.org/10.1016/j.ejmech.2019.04.074.

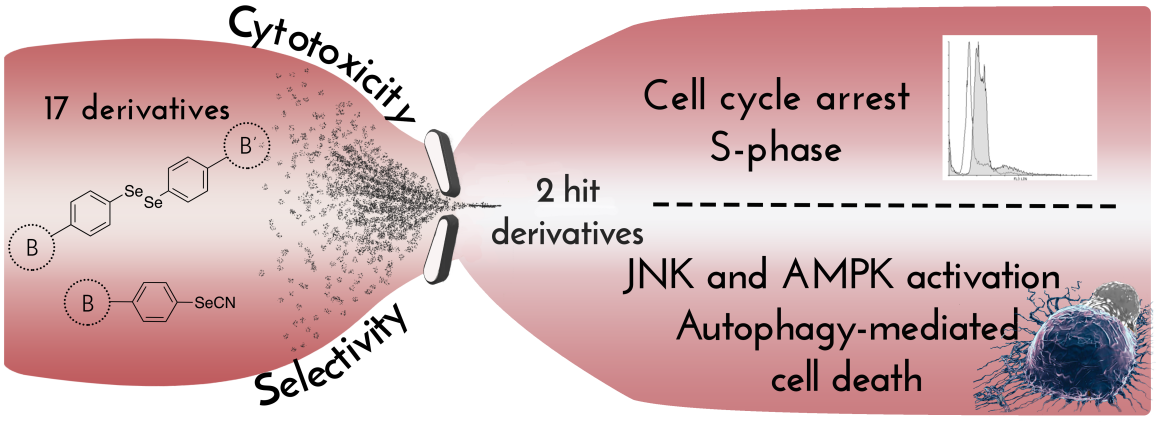

Organoseleno cytostatic derivatives: autophagic cell death with AMPK and JNK activation.

Pablo Garnica [1,2], Ignacio Encío [2,3], Daniel Plano [1,2], Juan A. Palop [1,2], Carmen Sanmartín [1,2]*

[1] Universidad de Navarra, Facultad de Farmacia y Nutrición, Departamento de Tecnología y Química Farmacéuticas. Campus Universitario, 31080, Pamplona, España
[2] Instituto de Investigación Sanitaria de Navarra (IdiSNA), Irunlarrea 3, E-31008 Pamplona, Spain
[3] Department of Health Sciences, Public University of Navarra, Avda. Barañain s/n, E-31008 Pamplona, Spain

* Prof. Carmen Sanmartín

Department of Pharmaceutical Technology and Chemistry

University of Navarra

Irunlarrea, 1, E-31008 Pamplona

SPAIN

+34 948 425 600 (Telephone)

+34 948 425 649 (Fax)

e-mail: sanmartin@unav.es

Abstract

Selenocyanates and diselenides are potential antitumor agents. Here we report two series of selenium derivatives related to selenocyanates and diselenides containing carboxylic, amide and imide moieties. These compounds were screened for their potency and selectivity against seven tumor cell lines and two non-malignant cell lines. Results showed that MCF-7 cells were especially sensitive to the treatment, with seven compounds presenting GI_{50} values below 10 μM. Notably, the carboxylic selenocyanate **8b** and the cyclic imide **10a** also displayed high selectivity for tumor cells. Treatment of MCF-7 cells with these compounds resulted in cell cycle arrest at S phase, increased levels of pJNK and pAMPK and caspase independent cell death. Autophagy inhibitors wortmannin and chloroquine partially prevented **8b** and **10a** induced cell death. Consistent with autophagy, increased Beclin1 and LC3-IIB and reduced SQSTM1/p62 levels were detected. Our results point to **8b** and **10a** as autophagic cell death inducers.

Keywords: Autophagy, cancer, cyclic imide, diselenide, selenocyanate.

1. Introduction

Despite recent advances in development of anticancer agents, this illness remains a leading cause of disease-related death worldwide [1]. Due to their effect on several survival or death signaling pathways that may decide the fate of cancer cells [2, 3], therapies based on autophagy targeted agents are now in the focus of a wide range of researchers. Among the signaling pathways implicated in these processes, JNK activation has been proven to participate in multiple autophagic events such as Beclin1 expression and autophagic-mediated cell death [4, 5]. Energetic stress has also been described to be a trigger for autophagy [6]; in this context, AMPK has been proven to have an essential role promoting autophagy by inhibiting the mTORs regulatory cascade [7]. The phosphorylation of AMPK and JNK in autophagy-mediated cell death has been previously described in breast adenocarcinoma [8, 9] and several other cancer types such as myeloma [10] and leukemia [11].

During the past decade, extensive studies of selenium compounds have demonstrated their antitumor and chemopreventive activities in a vast array of experimental models [12]. These derivatives interfere with the redox homeostasis and signaling of cancer cells. The mechanism by which they cause their effect include alterations in cell cycle checkpoints, proliferation, senescence, and death pathways [13]. In addition, some selenium derivatives such as selenite, selenocysteine and *Se*-allylselenocysteine play an effective role in cancer treatment as autophagy inducers and modulators of the JNK signaling pathway [14-17].

Many chemical entities containing selenium, with potent antitumor activity, have been explored by the scientific community. Among them, selenocyanate [18] and diselenide [19] moieties have been highlighted due to their interesting antitumor properties. In this line of investigation two effective derivatives, the diselenide analog bis(4-

aminophenyl)diselenide (**0a**) and the corresponding selenocyanate (**0b**), were recently identified in our laboratory [20]. In order to obtain a second generation of selenium structures with improved activity, selectivity and water solubility these compounds have been used as a starting point to continue with their modulation [21]. It is remarkable that one of the limitations of the selenium derivatives is their poor water solubility which is detrimental for their bioavailability and drug development. To obtain compounds with improved pharmacokinetic properties, modifications in the hydrophobic scaffold that improve water solubility are usually assayed. As an example of this strategy, introduction of a hydroxyl group in the phenyl ring of the natural product camptothecin has been shown to counteract efficiently this drawback [22]. Thus, a useful option when using this approach is to incorporate polar functional groups, such as acidic or basic groups. These fragments enable the possibility of salt formation and therefore might enhance water solubility [23, 24]. In this study, substantial efforts had been directed towards finding different chemical scaffolds that, while maintaining the cytotoxic activity, should increase the hydrophilicity further contributing to the solubility optimization. Among the structural features incorporated, we surmised that the introduction of the carboxylic core could be a logical approach for improving its aqueous solubility. This moiety is present in widely described organoselenium compounds such as 3,3'-diselenodipropionic acid [25]. In addition, the dicarboxylic acids are of special importance because of their versatility in the preparation of the corresponding cyclic imide homologs which are widely described in the literature as potential antitumor agents [26, 27].

Taking into consideration the facts stated above and our previous work in the field of new selenium compounds as antitumor agents [21, 28-33], the present study aimed to synthesize selenocyanates and diselenides containing carboxylic, amide and imide

moieties. The general outline of this series of compounds is presented in **Figure 1**. Variations were made in the group linked to the carboxy feature through selection of different cyclic symmetric anhydrides commercially available such as maleic, succinic, phthalic... Finally, with the objective of widening the structural variations, a new anhydride was synthesized through the Diels-Alder cycloaddition. The rationality behind this proposal is the synthesis of a structural analog of norcantharidin, a well-known active antitumor autophagy inducer [34].

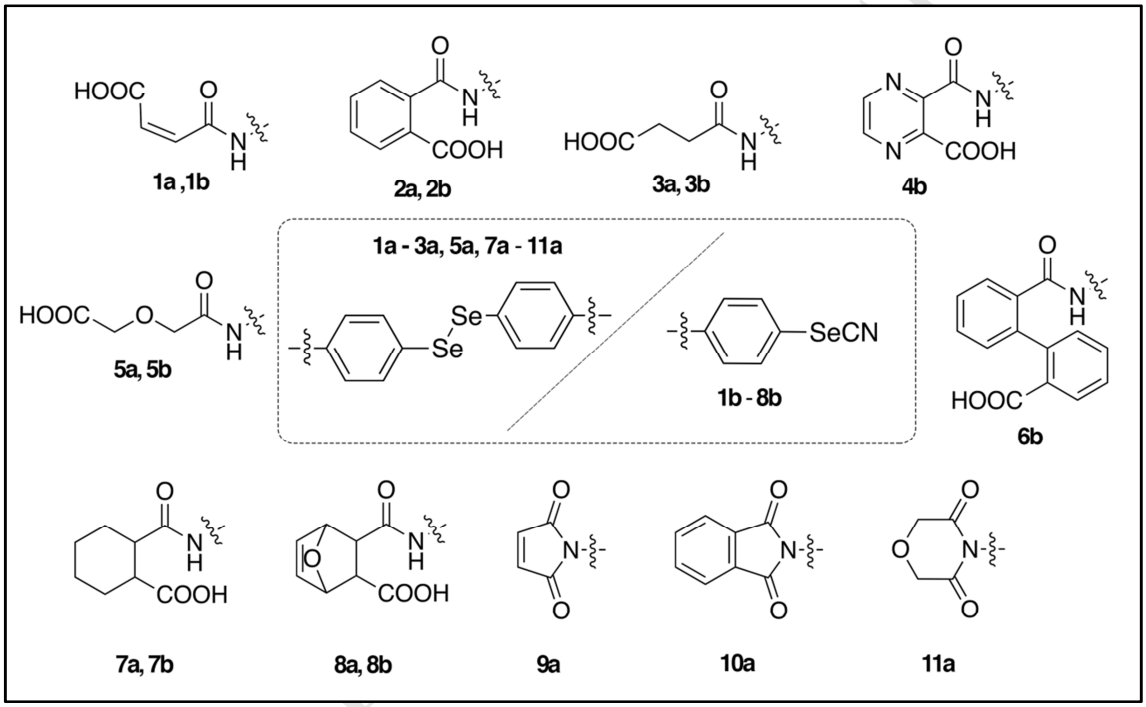

Figure 1. Structures of novel selenium containing compounds.

2. Results and discussion

2.1. Chemistry

The seventeen compounds synthesized and presented in this work can be categorized into two different subseries according to their selenium moiety:

- Diselenide derivatives containing carboxylic and amide or imide moieties (**1a-3a**, **5a**, **7a-11a**).
- Selenocyanate derivatives containing carboxylic and amide moieties (**1b-8b)**.

The resulting compounds were numbered according to the corresponding anhydride used as starting material.

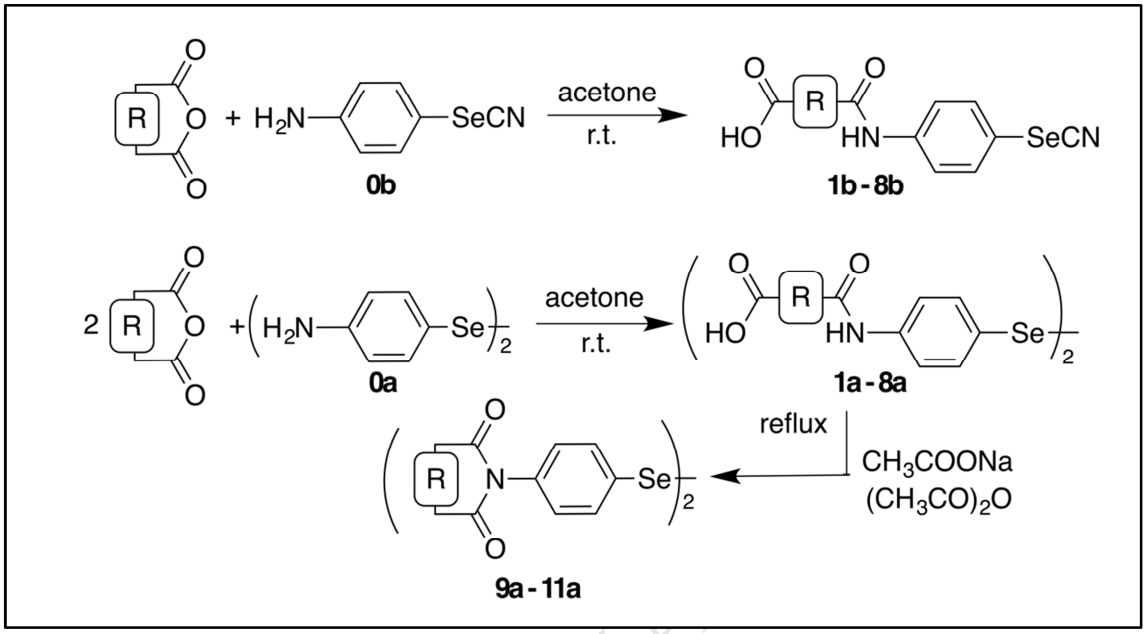

Figure 2. General procedure of synthesis.

Derivatives were synthesized following the synthetic path depicted in **Figure 2**. The corresponding anhydrides were reacted with either bis(4-aminophenyl)diselenide (**0a**) or 4-aminophenylselenocyanate (**0b**) in acetone at room temperature for 8 h up to 24 h. The formed precipitate was filtered and washed with *n*-hexane or ethyl ether to yield the final compounds. The mechanism proposed for this reaction is a nucleophilic acyl substitution illustrated in **Figure 3A**. Moreover, all our attempts to generate derivatives **4a** and **6a** were unsuccessful since the reaction of the corresponding anhydrides with **0a** in different conditions (temperature, solvents and catalyst) failed to yield the desired compound. Unfortunately, the alternative strategy of reducing their selenocyanate analogs (**4b** and **6b**) to obtain derivatives **4a** and **6a** under different conditions only resulted in the degradation of the start-up derivatives. To obtain the cyclic imides (**9a-11a**), the corresponding amidic acids (**1a, 2a, 5a**) were heated in presence of acetic

anhydride and sodium acetate. This reaction probably starts by a deprotonation of the carboxylic group, followed by the nucleophilic attack of the oxygen to the carbonyl group on the acetic anhydride followed by a subsequent intramolecular cyclization to yield the final cyclic imides. The reaction was quenched with water causing the prompt precipitation of the desired compound. The proposed mechanism of reaction to yield the cyclic imides is exemplified in **Figure 3B**.

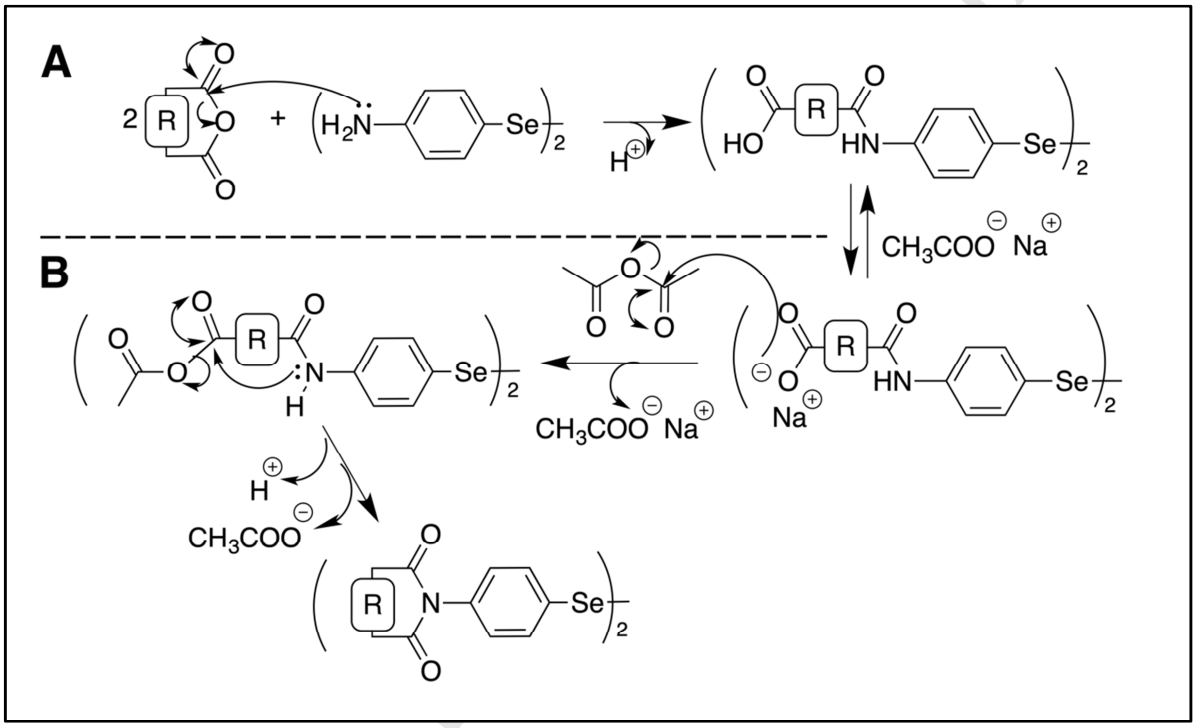

Figure 3. Mechanism proposed for the synthesis diselenide derivatives. Mechanism proposed for the synthesis of compounds **1a-3a**, **5a** and **7a-8a** (**A**). Mechanism proposed for the synthesis of cyclic imide derivatives **9a-11a** (**B**).

2.2. Biology

2.2.1. Cytotoxicity and antiproliferative activity

The cytotoxic potential of the seventeen synthesized compounds was evaluated against a panel of cell lines including seven different cancer cell lines and two other cell lines

derived from non-malignant tissue. Evaluation was performed at 48 h treatment following the MTT (3-(4,5-dimethylthiazol-2-yl)-2,5-diphenyltetrazolium bromide) methodology as previously described [33]. The cancer cell lines included in the panel were PC-3 (prostatic adenocarcinoma); HTB-54 (lung carcinoma), and HT-29 (colon carcinoma); MOLT-4 and CCRF-CEM (acute lymphoblastic leukemia); K-562 (chronic myelogenous leukemia) and MCF-7 (breast adenocarcinoma). The selected cell lines derived from non-malignant tissue were 184B5 and BEAS-2B. Cisplatin was used as positive control. In addition, the parent compounds bis(4-aminophenyl)diselenide (**0a**) and 4-aminophenylselenocyanate (**0b**) were tested as a reference to identify whether the second generation compounds accomplished the objective of improving potency and selectivity.

To narrow down the number of derivatives moving on to the full dose-response cytotoxic profiling assay, a two-dose concentration (100 μM and 10 μM) screening was first performed. The results obtained for the 10 μM treatment are shown in **Figure 4**. As shown in the figure, MCF-7 cells were the most sensitive cells toward the tested derivatives. In fact, seven compounds (**1b**, **2b**, **4b**, **8a**, **8b**, **9a** and **10a**) reduced cell growth to less than 50% when assayed at 10 μM in these cells. Some compounds also matched this threshold in PC-3, CCRF-CEM, HTB-54, MOLT-4 and HT-29 cells. However, none of the derivatives was able to reduce the cell growth effectively in K-562, the most resistant cell line to the treatments. Interestingly, compounds **1b**, **2b**, **4b**, **8a**, **8b**, **9a** and **10a** did not significantly affect cell growth in 184B5 cells, thus suggesting a potential selectivity of the compounds for breast cancer cells. Consequently, those seven compounds were further analysed in full dose-response curves in every cell line. GI_{50}, TGI and LC_{50} values were calculated form the curves and

are shown in **Table 1**. Selectivity for tumor cells was estimated according to the formulas GI_{50} (184B5)/GI_{50} (MCF-7) and GI_{50} (BEAS-2B)/GI_{50}(HTB-54) (**Table 2**).

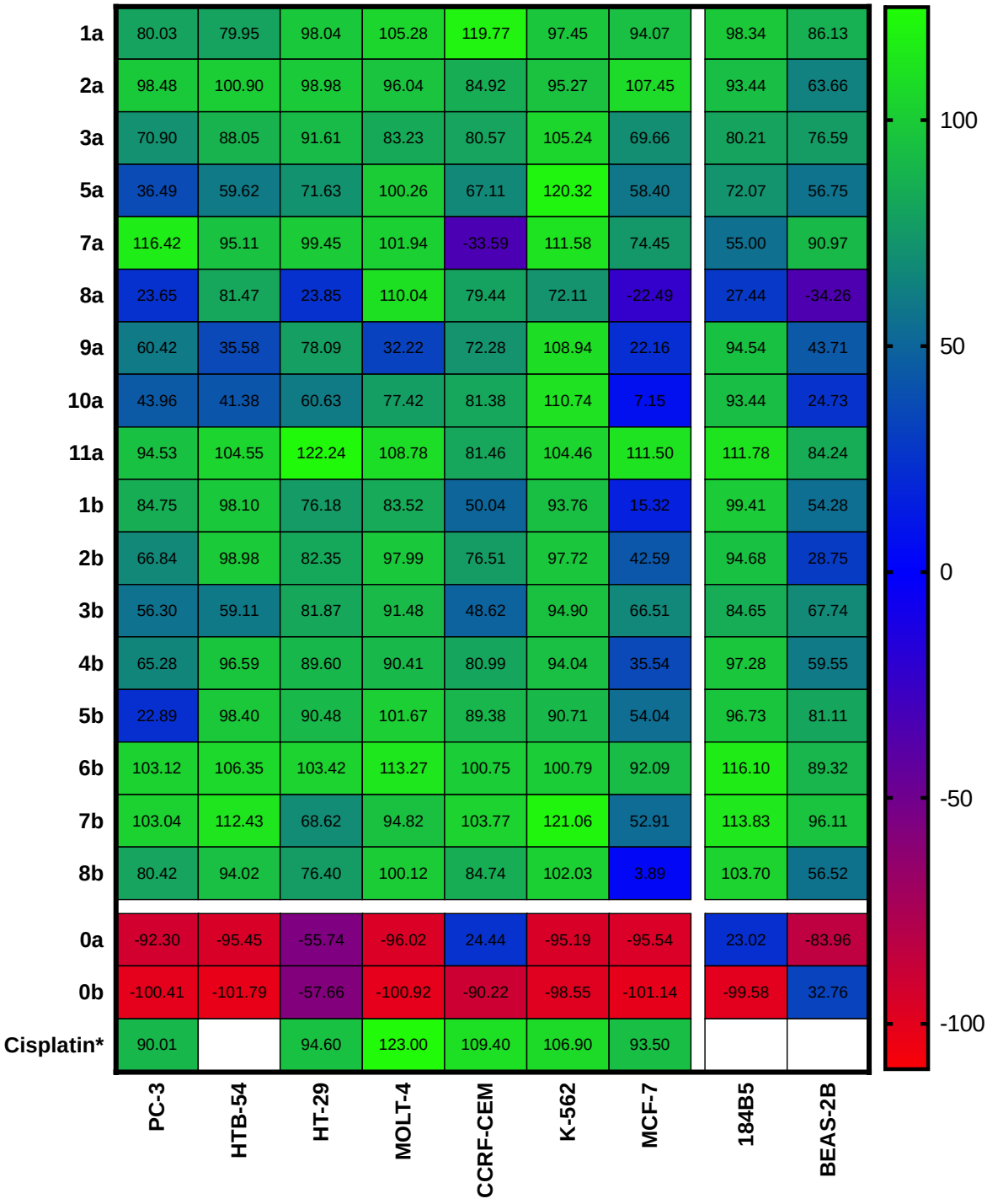

* NCI data (http://dtp.nci.nih.gov).

Figure 4. Heat map representing average percentages of cell growth for every tested structure at a 10 μM concentration for 48 h.

Table 1. Average values of GI_{50}, TGI and LD_{50} (μM) for 48 h treatment.

Code	PC-3			HTB-54			HT-29			MOLT-4			CCRF-CEM			K-562			MCF-7		
	GI_{50}[a]	TGI[b]	LD_{50}[c]	GI_{50}	TGI	LD_{50}	GI_{50}	TGI	LD_{50}	GI_{50}	TGI	LD_{50}	GI_{50}	TGI	LD_{50}	GI_{50}	TGI	LD_{50}	GI_{50}	TGI	LD_{50}
1b	30.44	61.35	92.89	46.95	72.42	93.75	>100	>100	>100	>100	>100	>100	6.77	38.33	91.19	58.58	98.17	>100	1.93	14.83	73.09
2b	19.38	>100	>100	>100	>100	>100	>100	>100	>100	>100	>100	>100	30.16	64.24	95.49	42.82	61.91	88.70	7.71	59.13	>100
4b	68.52	>100	>100	100	>100	>100	>100	>100	>100	>100	>100	>100	46.52	>100	>100	>100	>100	>100	6.47	>100	>100
8a	4.51	17.03	50.55	27.51	55.94	85.49	5.74	33.38	>100	73.77	84.71	94.62	59.13	75.84	>100	25.32	59.67	94.62	7.50	9.18	11.56
8b	21.05	43.22	70.44	47.83	72.42	>100	11.89	42.82	93.75	59.67	69.80	80.15	68.52	>100	>100	67.89	80.15	92.04	3.33	11.56	>100
9a	13.52	36.61	67.89	8.30	14.29	24.18	14.16	20.67	31.01	7.50	15.67	33.69	20.29	47.39	78.69	48.72	69.80	87.08	6.01	11.89	16.57
10a	8.30	33.08	>100	4.91	51.97	>100	11.67	>100	>100	91.19	>100	>100	>100	>100	>100	80.89	>100	>100	0.00096	7.64	>100
0b	1.02	1.54	2.30	0.87	1.00	1.13	0.27	1.11	5.28	3.33	3.39	3.42	1.71	2.74	4.43	1.03	1.29	1.58	1.00	1.48	2.20
0a	0.80	1.62	2.98	0.21	0.80	2.16	<0.01	1.78	8.37	3.84	5.95	8.06	5.28	16.87	42.82	0.95	1.19	1.48	0.75	0.96	1.16
Cisplatin *	5.01	50.1	>100	n.d.[#]	n.d.[#]	n.d.[#]	7.94	>100	>100	1.58	63.10	>100	1.00	79.43	>100	5.01	>100	>100	3.16	>100	>100

[a] GI_{50}, concentration that reduces growth by 50% compared to control. [b] TGI, concentration that completely inhibits cell growth. [c] LC_{50}, concentration that kills 50% of cells. [#] Not determined. * NCI data (http://dtp.nci.nih.gov).

Table 2. Average values of GI_{50}, TGI and LD_{50} (μM) for 48 h treatment and calculated SI.

Code	184B5			SI[a]	BEAS-2B			SI[b]
	GI_{50}	TGI	GI_{50}		GI_{50}	TGI	LD_{50}	
1b	>100	>100	>100	>51.73	10.45	42.82	80.15	0.22
2b	>100	>100	>100	>12.98	4.43	24.63	>100	<0.39
4b	>100	>100	>100	15.46	52.93	>100	>100	<0.16
8a	8.93	11.25	15.67	1.19	1.05	4.43	15.53	0.04
8b	77.25	91.19	>100	23.19	15.82	51.02	77.25	0.33
9a	40.51	63.07	86.29	6.74	1.97	43.62	73.77	0.24
10a	60.78	>100	> 100	6.3×10^4	0.75	20.86	61.91	0.15
0a	6.29	14.03	30.44	8.39	0.73	0.88	1.09	3.44
0b	0.88	1.06	1.27	0.88	7.92	14.69	27.51	9.06

[a] Selectivity index (SI) calculated as GI_{50} (184B5)/GI_{50} (MCF-7). [b] SI calculated as GI_{50} (BEAS-2B)/GI_{50}(HTB-54).

As shown in **Tables 1** and **2**, derivatives **8a**, **9a** and **10a** exhibited GI_{50} values under 10 μM in three of the tested cancer cell lines. Besides, compounds **1b**, **2b**, **4b, 8b** and **10a** were highly selective for tumor cells in the breast model. Remarkably, though highly cytotoxic, parent compounds **0a** and **0b** showed low selectivity for breast cancer cells (SI < 9). Therefore, we decided to focus on the effects of these compounds in the breast cancer cell line. When ranked in terms of potency and selectivity for breast cancer cells, a clear gap established **10a**, a compound with a nanomolar GI_{50} value and a staggering

SI, as the leader structure. Despite less cytotoxic, **1b** and **8b** were also highly selective. Among them, the analog derivative of norcantharidin (**8b**) was selected in order to evaluate whether this structure was able to mimic norcantharidin's effect and induce autophagy. As a result, derivatives **8b** and **10a** were selected to further analyse their mechanism of action in MCF-7 cells. As only the highest concentration tested led to negative growth values as exemplified on **Figure 5**, these results uncover a mainly cytostatic profile.

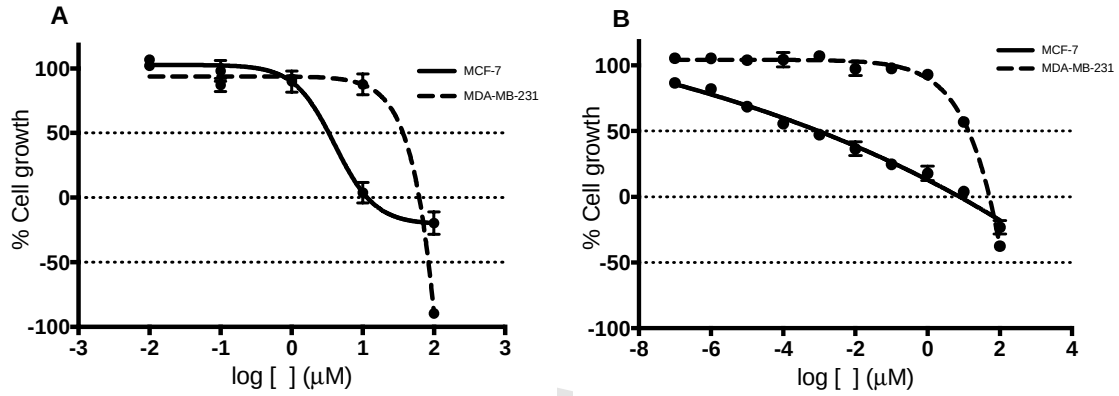

Figure 5. Dose response curves obtained for 8b (A) and 10a (B) in MCF-7 and MDA-MB-231 cell lines.

Besides, comparison between **10a** and **0a** clearly showed a great enhancement in selectivity for the second generation compound. In fact, SI was 7,000 times higher for compound **10a** than for **0a**, its parent compound. This effect was less notorious when compound **8b** was compared with **0b**. However, both **10a** and **8b** succeeded in increasing the selectivity towards the cancer cells, thus meeting one of our goals.

The importance of estrogen receptors (ER) in cell cycle and cell proliferation in breast cancer cells, as well as the crucial role of estradiol synthesis pathways has been widely described. In fact, antiestrogens have been found to repress transcription of several ERα target genes in MCF-7 cells, specifically in S phase [35]. Besides, when MCF-7 cell

cultures were exposed to a genotoxic agent higher levels of DNA damage in *S*- and *G2/M*-enriched cultures correlated with higher levels of CYP1A1 y CYP1B1 [36]. MCF-7 is an ERα expressing cell line. Therefore, to compare we decided to test **8b** and **10a** in MDA-MB-231, a breast cancer cell line non-expressing ERα. Obtained results for MDA-MB-231 cells are shown in **Figure 5**. As shown in the figure, **8a** and **10a** dose-response curves in MDA-MB-231differ from those obtained in MCF-7 cells. Moreover, lying in the micromolar range GI_{50}, TGI and LD_{50} values for **8b** (GI_{50}= 33.61 μM, TGI= 61.92 μM and LD_{50}= 83.92 μM) and **10a** (GI_{50}= 13.65 μM, TGI= 51.49 μM and LD_{50}> 100 μM) are also higher than in MCF-7cells. These data suggest that ER signalling and/or estradiol metabolism play a relevant role in cytostatic effect displayed by **8b** and **10a** in MCF-7 cells.

In terms of structure-activity relationship, most diselenide structures containing carboxylic moieties were discarded in the screening process. For instance, when comparing **8b** with its diselenide homolog a complete loss of selectivity could be observed. On the other hand, if we stablish a comparison between carboxylic derivatives and their cyclic imide homologs data suggests that this modification was crucial for both potency and selectivity.

*2.2.2. Compounds **8b** and **10a** induce cell cycle arrest in S phase and cell death*

Many selenium containing compounds involve cell cycle regulation among their therapeutic effects [13]. Therefore, as a first approach to the mechanism of action we studied the effect of **8b** and **10a** on cell cycle. With this purpose, the cell cycle status of MCF-7 cell cultures treated with different concentrations of **8b** and **10a** and for different time points was determined by flow cytometry. Camptothecin was used as positive control. As shown in the **Figure 6**, both a reduction in the number of G_0/G_1 cells and a significant increase in the percentage of cells in S phase were detected for

both compounds even at the lowest concentration (10 μM) and the shortest time tested (24 h). This result, indicative of S phase arrest was both dose (**Figure 6A**) and time (**Figures 6B** and **C**) dependent.

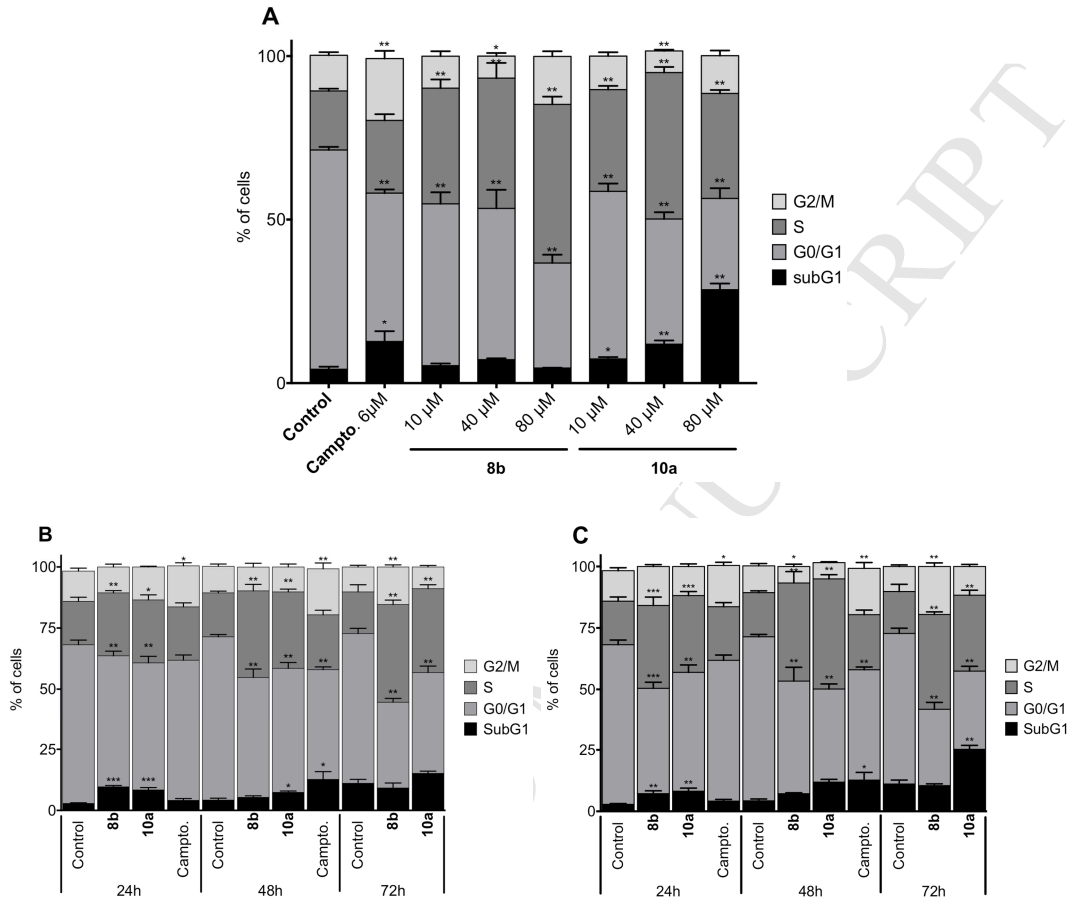

Figure 6. Cell cycle phase distribution of MCF-7 cell cultures after treatment with compounds 8b and 10a. (**A**) Dose-dependent induction of cell cycle arrest after 48 h treatment with compounds **8b** and **10a**. Time-course analysis of cell cycle distribution at 10 μM (**B**) and 40 μM (**C**) of **8b** and **10a**. Camptothecin (6 μM) was employed as a positive control. Results are expressed as a mean ± SEM of at least three independent experiments performed in duplicate. *$p < 0.05$, **$p < 0.01$ and ***$p < 0.001$ compared to control cells.

To study the role of apoptosis in the induction of cell death by **8b** and **10a**, MCF-7 cells were incubated in the presence of increasing concentrations of **8b** and **10a** for 48 h. Then, the apoptotic status of the cells was studied by TUNEL. As shown in **Figure 7A**, when tested at concentrations higher than 40 μM, both compounds induced a significant increase in the number of death cells (subdiploid cells). **Figure 7B** shows that at 40 μM concentration the induction of cell death could be detected as soon as 24 h.

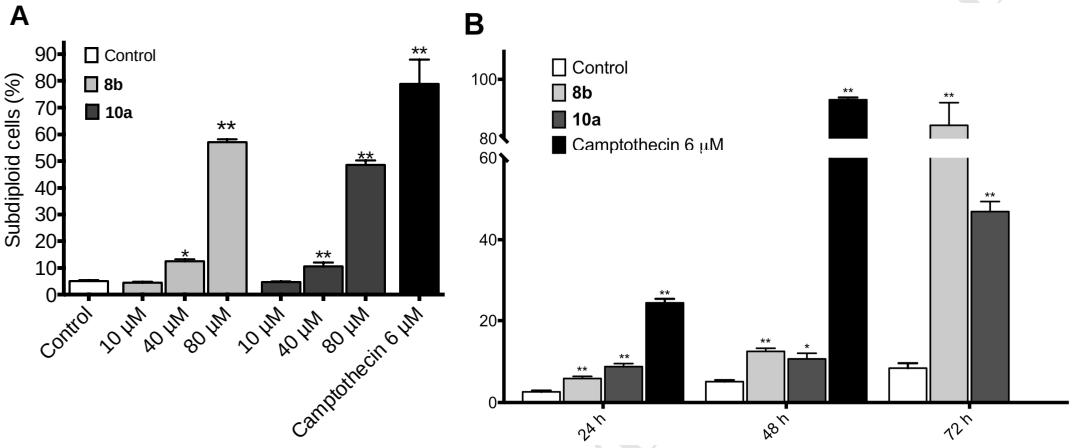

Figure 7. Compounds 8b and 10a induced cell death in a dose- and time-dependent manner in MCF-7 cell cultures. Cells were treated with increasing concentrations of compounds **8b** and **10a** for 48 h (**A**) or at 40 μM concentration for different periods of time (**B**). Camptothecin was used as positive control. Results are expressed as a mean ± SEM of at least three independent experiments performed in duplicate. *$p < 0.05$ and **$p < 0.01$ compared to control cells.

*2.2.3. Compounds **8b** and **10a** induce autophagy-mediated cell death and AMPK/JNK pathway activation*

To further analyse the molecular mechanism by which **8b** and **10a** reduced MCF-7 cell viability, we explored the effect of pre-treatment of the cultures with either an autophagy inhibitor (wortmannin, chloroquine) [37-39] or a pan-caspase inhibitor (Z-

VAD-FMK) on the induction of cell death by these compounds. As shown in **Figure 8**, pre-treatment of the cells with the PI3K inhibitor wortmannin or the lysosomal inhibitor chloroquine led to a significant reduction in the number of dead cells in the cultures after exposure to compounds **8b** and **10a**. However, pre-incubation of the cultures with Z-VAD-FMK could not prevent **8b** and **10a**-induced cell death. These results suggest that autophagy is the way by which **8b** and **10a** cause their effect.

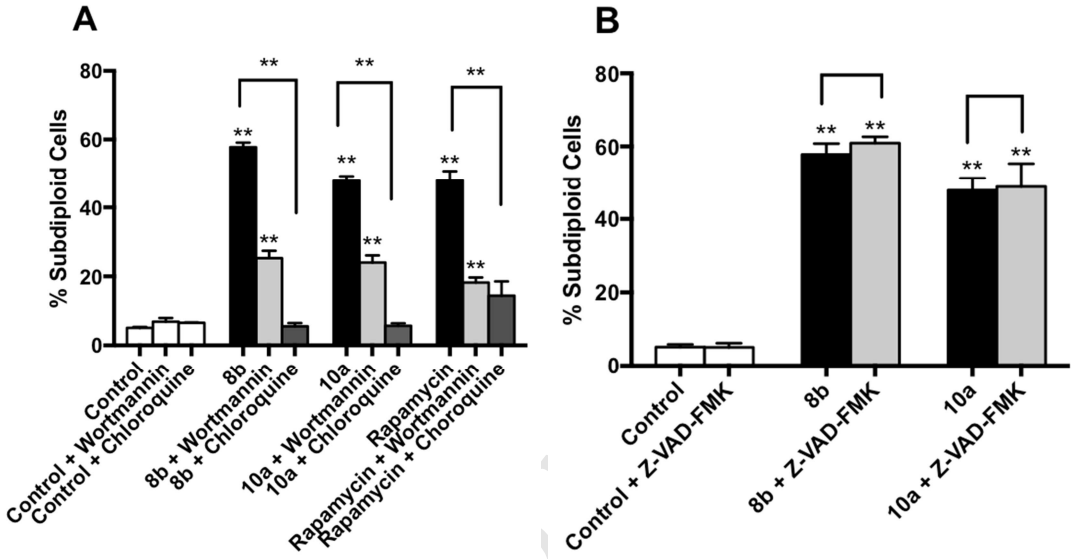

Figure 8. Cell death induced by compounds 8b and 10a is partially blocked by wortmannin or chloroquine but not by caspase inhibitor Z-VAD-FMK. Cell death determination in MCF-7 cell cultures pre-incubated with (**A**) 100 nM wortmannin, 10 μM chloroquine or (**B**) 50 mM Z-VAD-FMK before treatment with 80 μM **8b**, 80 μM **10a** or 30 μM rapamycin for 48 h. Rapamycin was used as reference autophagy control at 30 μM treatment. Results are expressed as a mean ± SEM of at least three independent experiments performed in duplicate. *$p < 0.05$ and **$p < 0.01$ compared to the control.

To further confirm the involvement of autophagy in **8b** and **10a** induced cell death the levels of expression of the autophagy markers Beclin-1 and LC3B were determined. Autophagic flux was also assessed by testing SQSTM1/p62 [40]. As shown in **Figure 9**, when MCF-7 cells were treated with 80 μM of either compound for 48 h, Beclin-1, LC3B-I and LC3B-II were augmented while SQSTM1/p62 was downregulated thus confirming autophagy. Since the activation of AMPK and JNK have been shown to play a role in autophagy-mediated cell death [6, 41], AMPK and JNK phosphorylation were also studied. As shown in **Figure 9**, both **8b** and **10a** induced AMPK and JNK phosphorylation.

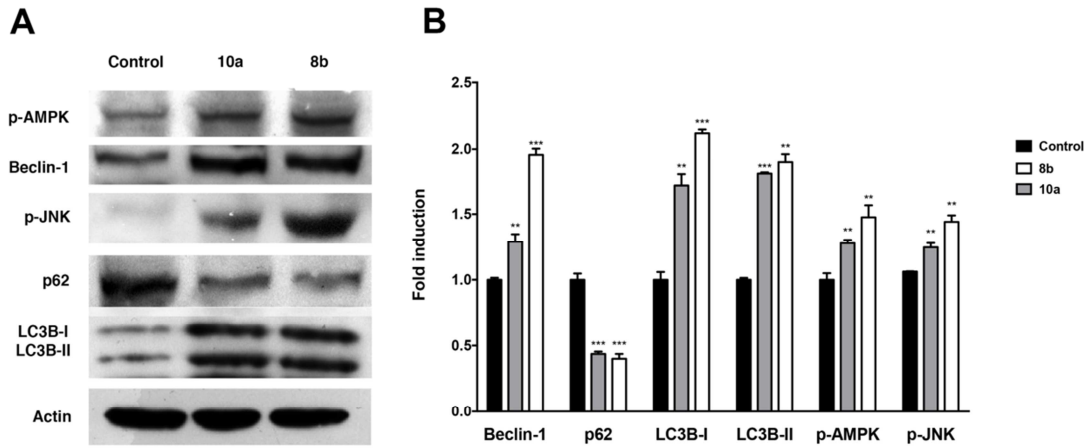

Figure 9. Beclin-1, p62, LC3B-I, LC3B-II, p-AMPK and p-JNK proteins were determined by western blot. (**A**) A representative experiment is exemplified. (**B**) Aggregate results (mean ± SEM; n=3) expressed as fold induction relative to control cells. *$p < 0.05$, **$p < 0.01$ and ***$p < 0.001$.

Inhibition of mTORC1 after AMPK activation is a main step in AMPK-mediated autophagy. The PI3K/AKT pathway also has a regulatory effect on mTOR and therefore in autophagy. This pathway is commonly deregulated in cancer cells [42]. Aimed to

analyze the effect of **8b** and **10a** on PI3K and AKT signaling, we determined the phosphorylation status of both, the PI3K catalytic subunit p110α and AKT (Ser473). As shown in **Figure 10**, increased phospho-p110α and phospho-AKT (Ser473) were detected indicating activation of the pathway. PI3K activation is usually related to tumor migration enhancement [43] and has been reported to be associated with inhibition of autophagy and tumorgenesis [44]. However, in the specific context of breast adenocarcinoma cells PI3K activation does not necessarily lead to autophagy suppression [45]. Moreover, specific activation of the isoform 1 of AKT in breast, neck and head carcinomas has been shown to interfere with their metastatic progression [46, 47]. Whether AKT-mediated repression of metastasis would represent an additional beneficial effect of the treatment with compounds **8b** and **10a** merits further research.

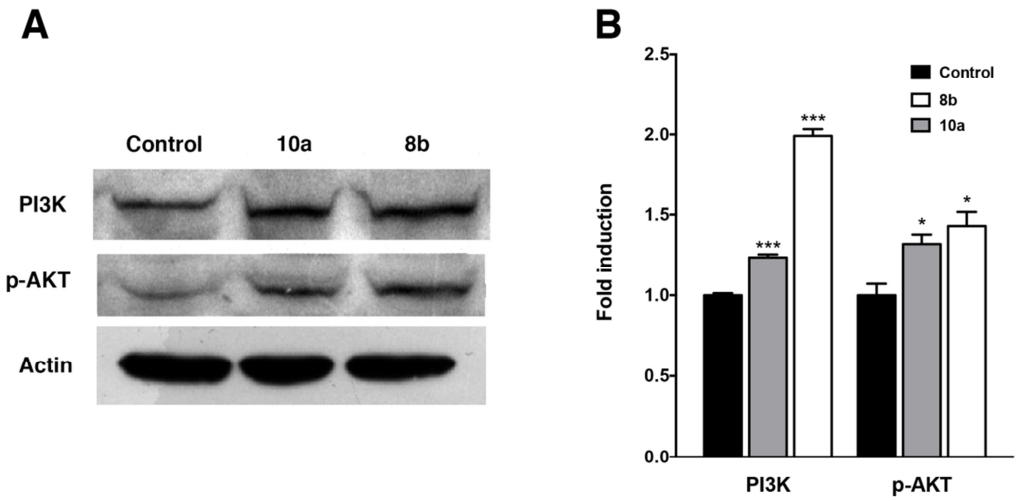

Figure 10. PI3K and p-AKT proteins were determined by western blot. (**A**) A representative experiment is exemplified. (**B**) Aggregate results (mean ± SEM; n=3) expressed as fold induction relative to control cells. *p < 0.05, **p < 0.01 and ***p < 0.001.

3. Conclusion

To sum up, nine diselenide (**1a**-**3a**, **5a**, **7a**-**11a**) and eight selenocyanate monoamidic acids (**1b**-**8b**) were synthesized with high yields. A screening in a panel of cancer cell lines revealed that MCF-7 was the most sensitive among the tested ones to treatment with these compounds. Due to their high potency and stunning selectivity towards MCF-7 cells, derivatives **8b** and **10a** emerged as the most promising structures. Full dose response curves in MCF-7 cells showed up a cytostatic effect for these compounds. Further analysis uncovered their ability to induce both S phase arrest and a caspase-independent cell death program in these cells. Besides, wortmannin and chloroquine partially prevented induction of cell death, thus suggesting autophagy. Increased levels of Beclin1 and LC3-IIB and reduced levels of SQSTM1/p62 in MCF-7 cells after exposure to **8b** or **10a** also supported autophagy. Since pJNK upregulation and AMPK phosphorylation were also detected after the treatments, the modulation of the AMPK and JNK signaling pathways seems to be involved in the induction of autophagy by **8b** and **10a**. Finally, the phosphorylation of both, AKT and the PI3K catalytic subunit p110α were also detected. Whether the activation of the PI3K/AKT pathway by **8b** and **10a** in MCF-7 cells restricts their invasive capacity and represents an extra beneficial effect of these compounds for cancer treatment deserves to be studied profoundly.

4. Experimental

4.1. Chemistry

4.1.1. Material and methods

Proton (^{1}H) and carbon (^{13}C) NMR spectra of every compound and selenium (^{77}Se) NMR spectra of representative derivatives were recorded on a Bruker Advance Neo 400

Ultrashield™ spectrometer (Rheinstetten, Germany) using DMSO-d_6 as solvent. IR spectra were recorded on a Thermo Nicolet FT- IR Nexus spectrophotometer using KBr pellets for solid samples. Elemental analysis was performed on a LECO CHN-900 Elemental Analyzer. Purity of all final compounds was 95% or higher. Chemicals were purchased from E. Merck (Darmstadt, Germany), Panreac Química S.A. (Montcada i Reixac, Barcelona, Spain), Sigma-Aldrich Quimica, S.A. (Alcobendas, Madrid, Spain) and Acros Organics (Janssen Pharmaceuticalaan, Geel, Belgium).

4.1.2. General procedure for the synthesis of compounds ***1a-3a****,* ***5a*** *and* ***7a-8a***

Bis(4-aminophenyl)diselenide (1 mmol) was dissolved in of dry acetone (10 mL) and the corresponding anhydride (2.1 mmol) then added. The reaction was then stirred for a variable time of 8 h up to 24 h at room temperature. Then reaction was quenched with water, compound was filtered and purified by stirring or washing with ethyl ether.

In order to assign the chemical shifts in NMR spectroscopy the following assignment has been done: central rings A and A', external fragments B and B' (**Figure 10**).

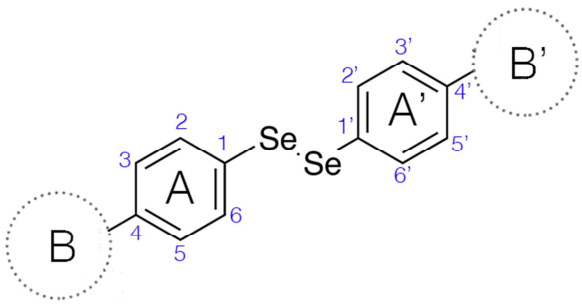

Figure 10. General NMR assignation for compounds of series a.

4.1.2.1. (2Z,2'Z)-4,4'-[diselenodiylbis(benzene-4,1-diylimino)]bis(4-oxobut-2-enoic acid) ***(1a)***

From maleic anhydride. Conditions: 8 h at room temperature. The product was kept under stirring with water (25 mL) for 2 h, filtered and then washed with ethyl ether (2 × 25 mL). A yellow powder was obtained. Yield: 68.9%. Mp: 186–186.5ºC. IR (KBr) cm^{-1}: 3305, 3193 (N-H), 1723 (C=O carboxylic acid), 1623 (C=O, amide), 818 (Se-Se). ^{1}H NMR (400 MHz, DMSO-d_6) δ: 13.01 (bs, 2H, COOH), 10.54 (s, 2H, NH), 7.60 (d, 4H, A+A', J_{2-3}=J_{6-5}= 8.8 Hz, H_2+H_6), 7.57 (d, 4H, A+A', J_{3-2}=J_{5-6}= 8.8 Hz, H_3+H_5), 6.46 (d, 2H, B+B', J_{1-2}= 12.0 Hz, H_1), 6.31 (d, 2H, B+B', J_{2-1}= 12.0 Hz, H_2). ^{13}C NMR (100 MHz, DMSO-d_6) δ: 166.76 (COOH), 163.17 (C=O), 138.71 (A+A', C_4), 132.88 (A+A', C_2+C_6), 131.33+130.23 (B+B', C_1+C_2), 124.19 (A+A', C_1), 120.02 (A+A', C_3+C_5). MS [*m/z* (% abundance)]: 172 (100), 344 (25). Elemental analysis calculated (%) for $C_{20}H_{16}N_2O_6Se_2 \cdot 2H_2O$: C: 41.83, H: 3.51, N: 4.88; found: C: 41.54, H: 3.53, N: 4.80.

*4.1.2.2. 2,2'-[(Diselenodiyldibenzene-4,1-diyl)dicarbamoyl]bis(benzoic acid) (**2a**)*

From phthalic anhydride. Conditions: 12 h at room temperature. The product was kept under stirring with water (25 mL) for 1 h, filtered and then washed with ethyl ether (2 × 25 mL). A yellow powder was obtained. Yield: 26.7%. Mp: 154–155ºC. IR (KBr) cm^{-1}: 3282 (N-H),1708 (C=O carboxylic acid), 1657 (C=O, amide), 819 (Se-Se). ^{1}H NMR (400 MHz, DMSO-d_6) δ: 11.02 (s, 2H, NH), 7.85 (d, 2H, B+B', J_{3-4}= 8.8 Hz, H_3), 7.72–7.66 (m, 4H, B+B', H_4+H_6), 7.63–7.52 (m, 10H, A+A', H_2+H_3+H_4+H_5, B+B', H_5), 3.39 (bs, H_2O+2COOH). ^{13}C NMR (100 MHz, DMSO-d_6) δ: 171.22 (COOH), 168.50 (C=O), 140.48 (A+A', C_4), 134.06+132.02 (A+A', C_2+C_6+C_1), 130.40+130.27 (B+B', C_5+C_4), 128.65+126.48 (B+B', C_1+C_2), 124.60 (A+A', C_3+C_5), 121.03+120.51 (B+B', C_3+C_6). ^{77}Se NMR (76 MHz, DMSO-d_6) δ: 482.83 (Se-Se). MS [*m/z* (% abundance)]: 104 (100), 172 (93), 344 (25). Elemental analysis calculated (%) for $C_{28}H_{20}N_2O_6Se_2 \cdot 2H_2O$: C: 49.87, H: 3.59, N: 4.15; found: C: 49.73, H: 3.53, N: 4.35.

*4.1.2.3. 4,4'-[Diselenodiylbis(benzene-4,1-diylimino)]bis(4-oxobutanoic acid) (**3a**)*

From succinic anhydride. Conditions: 24 h at room temperature. The product was kept under stirring with water (25 mL) for 2 h, filtered, then stirred with ethyl ether (100 mL) for 24 h and then filtered. A yellow powder was obtained. Yield: 72.27%. Mp: 179–180ºC. IR (KBr) cm^{-1}: 3318 (NH), 1696 (C=O carboxylic acid), 1666 (C=O, amide), 818 (Se-Se). ^{1}H NMR (400 MHz, DMSO-d_6) δ: 12.21 (bs, 2H, COOH), 10.11 (s, 2H, NH), 7.56 (d, 4H, A+A', J_{2-3}= J_{6-5}= 8.4 Hz, H_2+H_6), 7.51 (d, 4H, A+A', J_{3-2}= J_{5-6}= 8.4 Hz, H_3+H_5), 2.60–2.46 (m, 8H, B+B', H_1+H_2). ^{13}C NMR (100 MHz, DMSO-d_6) δ: 174.27 (COOH), 170.80 (C=O), 140.09 (A+A', C_4), 133.76 (A+A', C_2+C_6), 123.85 (A+A', C_1), 120.12 (A+A', C_3+C_5), 31.57+29.23 (B+B', C_2+C_1). MS [*m/z* (% abundance)]: 172 (100), 344 (15), 424 (10). Elemental analysis calculated (%) for $C_{20}H_{20}N_2O_6Se_2 \cdot 2H_2O$: C: 41.51, H: 4.18, N: 4.84; found: C: 41.11, H: 3.79, N: 4.77.

*4.1.2.4. 2,2'-[(Diselenodiylbis(benzene-4,1-diylimino)]bis(2-oxoethane-2,1-diyloxy)diacetic acid (**5a**)*

From diglycolic anhydride. Conditions: 24 h at room temperature. The product was kept under stirring with water (25 mL) for 2 h, filtered, then stirred with ethyl ether (100 mL) for 24 h and then filtered. A yellow powder was obtained. Yield: 69.7%. Mp: 140–141ºC. IR (KBr) cm^{-1}: 3337 (NH), 1709 (C=O carboxylic acid), 1683 (C=O, amide), 818 (Se-Se). ^{1}H NMR (400 MHz, DMSO-d_6) δ: 12.76 (bs, 2H, COOH), 10.09 (s, 2H, NH), 7.62 (d, 4H, A+A', J_{2-3}= J_{6-5}= 8.5 Hz, H_2+H_6), 7.55 (d, 4H, A+A', J_{3-2}= J_{5-6}= 8.5 Hz, H_3+H_5), 4.19 (s, 4H, B+B', H_1), 4.17 (s, 4H, B+B', H_2). ^{13}C NMR (100 MHz, DMSO-d_6) δ: 172.68 (COOH), 168.99 (C=O), 139.56 (A+A', C_4), 133.94 (A+A', C_2+C_6), 125.01 (A+A', C_1), 121.22 (A+A', C_3+C_5), 71.38+69.11 (B+B', C_2+C_1). MS

[*m/z* (% abundance)]: 93 (95), 172 (100). Elemental analysis calculated (%) for $C_{20}H_{20}N_2O_8Se_2$: C: 41.83, H: 3.51, N: 4.88; found: C: 41.83, H: 3.82, N: 5.19.

*4.1.2.5. 2,2'-[(Diselenodiyldibenzene-4,1-diyl)dicarbamoyl]bis(cyclohexanecarboxylic acid) (**7a**)*

From *cis*-1,2-cyclohexanecarboxylic anhydride. Conditions: 24 h at room temperature. The product was kept under stirring with water (25 mL) for 2 h, filtered, then stirred with ethyl ether (100 mL) for 24 h and then filtered. A light brown powder was obtained. Yield: 97.7%. Mp: 150–151ºC. IR (KBr) cm^{-1}: 3307 (NH), 1698 (C=O carboxylic acid), 1665 (C=O, amide), 820 (Se-Se). ^{1}H NMR (400 MHz, DMSO-d_6) δ: 11.88 (bs, 2H, COOH), 9.87 (s, 2H, NH), 7.55 (d, 4H, A+A', $J_{2\text{-}3}$=$J_{6\text{-}5}$= 8.8 Hz, H_2+H_6), 7.50 (d, 4H, A+A', $J_{3\text{-}2}$=$J_{5\text{-}6}$= 8.8 Hz, H_3+H_5), 2.93 (d, 2H, B+B', $J_{1\text{-}CHchex}$= 5.4 Hz, H_1), 2.70–2.56 (m, 2H, B+B', H_{chex}), 2.09 (d, 2H, B+B', $J_{CHchex\text{-}1}$ = 5.4 Hz, H_{chex}), 1.98 (d, 2H, B+B', *J*= 8.9 Hz, H_{chex}), 1.83–1.57 (m, 6H, B+B', 3H_{chex}), 1.48–1.24 (m, 6H, B+B', 3H_{chex}). ^{13}C NMR (100 MHz, DMSO-d_6) δ: 175.56 (COOH), 173.36 (C=O), 140.42 (A+A', C_4), 133.78 (A+A', C_2+C_6), 123.66 (A+A', C_1), 120.26 (A+A', C_3+C_5), 43.00+42.44 (B+B', C_1+C_2), 28.13+25.62+24.47+22.78 (B+B', C_3+C_4+C_5+C_6). MS [*m/z* (% abundance)]: 81 (70), 172 (100), 344 (25). Elemental analysis calculated (%) for $C_{28}H_{32}N_2O_6Se_2$: C: 51.70, H: 4.96, N: 4.31; found: C: 52.06, H: 5.09, N: 4.71.

*4.1.2.6. 3,3'-[(Diselenodiyldibenzene-4,1-diyl)dicarbamoyl]bis(7-oxabicyclo[2.2.1]hept-5-ene-2-carboxylic acid) (**8a**)*

From 3,6-epoxy-1,2,3,6-tetrahydrophthalic anhydride obtained by the classic procedure described for a Diels-Alder reaction using furan and maleic anhydride as reagents to yield the Diels-Alder adduct. Conditions: 24 h at room temperature. The product was

kept under stirring with water (25 mL) for 2 h, filtered, then stirred with ethyl ether (100 mL) for 24 h and then filtered. A yellow powder was obtained. Yield: 22.5%. Mp: 126–127ºC IR (KBr) cm^{-1}: 3299 (NH), 1706 (C=O carboxylic acid), 1669 (C=O, amide), 819 (Se-Se). ^{1}H NMR (400 MHz, DMSO-d_6) δ: 12.19 (bs, 2H, COOH), 10.03 (s, 2H, NH), 7.65 (d, 4H, A+A', $J_{2\text{-}3}$=$J_{6\text{-}5}$= 9.0 Hz, H_2+H_6), 7.62 (d, 4H, A+A', $J_{3\text{-}2}$=$J_{5\text{-}6}$= 9.0 Hz, H_3+H_5), 6.50 (s, 4H, B+B', H_3+H_5), 5.14 (s, 2H, B+B', H_5), 5.06 (s, 2H, B+B', H_2), 2.82 (d, 2H, B+B', $J_{1\text{-}6}$= 9.1 Hz, H_1), 2.71 (d, 2H, B+B', $J_{6\text{-}1}$= 9.1 Hz, H_6). ^{13}C NMR (100 MHz, DMSO-d_6) δ: 173.08 (COOH), 170.48 (C=O), 141.07 (A+A', C_4), 137.49+137.08 (B+B', C_4+C_5), 135.29 (A+A', C_2+C_6), 120.79 (A+A', C_1), 116.51 (A+A', C_3+C_5), 80.82+79.61 (B+B', C_3+C_6), 47.96+47.36 (B+B', C_1+C_2). MS [*m/z* (% abundance)]: 172 (100), 344 (25). Elemental analysis calculated (%) for $C_{28}H_{24}N_2O_8Se_2 \cdot 2H_2O$: C: 47.34, H: 3.97, N: 3.94; found: C: 47.66, H: 4.13, N: 4.23.

*4.1.3. General procedure for the synthesis of compounds **9a–11a***

A reaction mixture containing 1.3 mmol of the corresponding carboxylic derivatives (**1a**, **2a** or **5a**) in 15 mL of acetic anhydride and 200 mg of sodium acetate was heated for 3 h under reflux, then quenched with water (50 mL) and kept under stirring for 3 h. The aqueous solution was extracted with CH_2Cl_2 (2 × 25 mL), dried with sodium sulphate anhydrous and the solvent was evaporated under vacuum.

*4.1.3.1. 1,1'-(Diselenediyldibenzene-4,1-diyl)bis(1H-pyrrole-2,5-dione) (**9a**)*

From compound **1a**. The product was then washed with *n*-hexane (100 mL). A yellow solid was obtained. Yield: 55.4%. Mp: 91.5–92.5ºC. IR (KBr) cm^{-1}: 1710 (C=O), 818 (Se-Se). ^{1}H NMR (400 MHz, DMSO-d_6) δ: 7.77 (d, 4H, A+A', $J_{2\text{-}3}$=$J_{6\text{-}5}$= 8.6 Hz, H_2+H_6), 7.33 (d, 4H, A+A', $J_{3\text{-}2}$=$J_{5\text{-}6}$= 8.6 Hz, H_3+H_5), 7.19 (s, 4H, B+B', H_1+H_2). ^{13}C

NMR (100 MHz, DMSO-d_6) δ: 169.69 (C=O), 134.75 (A+A', C_4), 131.37+131.27 (A+A', C_2+C_6; B+B', C_1+C_2), 129.15 (A+A', C_1), 127.51 (A+A', C_3+C_5). MS [m/z (% abundance)]: 57 (75), 252 (100), 311 (65). Elemental analysis calculated (%) for $C_{20}H_{12}N_2O_4Se_2 \cdot H_2O$: C: 46.17, H: 2.71, N: 5.38; found: C: 46.10, H: 3.03, N: 4.94.

*4.1.3.2. 1,1'-(Diselenodiyldibenzene-4,1-diyl)bis(1H-isoindole-1,3(2H)-dione) (**10a**)*

From compound **2a**. The product was then washed with *n*-hexane (100 mL). A yellow solid was obtained. Yield: 90.6%. Mp: 248–249ºC. IR (KBr) cm^{-1}: 1709 (C=O), 815 (Se-Se). ^{1}H NMR (400 MHz, DMSO-d_6) δ: 8.15–7.79 (m, 12H, A+A', H_2+H_6; B+B', H_2+H_3+H_4+H_5), 7.55 (d, 4H, A+A', $J_{3\text{-}2}$=$J_{5\text{-}6}$= 8.4 Hz, H_3+H_5). ^{13}C NMR (100 MHz, DMSO-d_6) δ: 172.73 (C=O), 140.18+140.09 (A+A', C_4; B+B', C_1+C_6), 133.49 (B+B', C_4+C_5), 131.99+131.73 (A+A', C_1+C_2+C_6), 128.65 (B+B', C_2+C_5), 120.26 (A+A', C_3+C_5). ^{77}Se NMR (76 MHz, DMSO-d_6) δ: 481.88 (Se-Se). MS [*m/z* (% abundance)]: 93 (65), 172 (100), 302 (15), 604 (5). Elemental analysis calculated (%) for $C_{28}H_{16}N_2O_4Se_2 \cdot 2H_2O$: C: 52.68, H: 3.16, N: 4.39; found: C: 52.82, H: 3.20, N: 4.77.

*4.1.3.3. 1,1'-(Diselenodiyldibenzene-4,1-diyl)bis(morpholine-3,5-dione) (**11a**)*

From compound **5a**. The product was then washed with ethyl ether (3 × 10 mL). A yellow solid was obtained. Yield: 72.6%. MP: 150–152. IR (KBr) cm^{-1}: 1708 (C=O), 819 (Se-Se). ^{1}H NMR (400 MHz, DMSO-d_6) δ*:* 7.76 (d, 4H, A+A', $J_{2\text{-}3}$=$J_{6\text{-}5}$= 7.8 Hz, H_2+H_6), 7.23 (d, 4H, A+A', $J_{3\text{-}2}$=$J_{5\text{-}6}$= 7.8 Hz, H_3+H_5), 4.54 (s, 8H, B+B', H_2+H_3). ^{13}C NMR (100 MHz, DMSO-d_6) δ: 170.19 (C=O), 133.32 (A+A', C_4), 131.42 (A+A', C_2+C_6), 130.71 (A+A', C_1), 130.30 (A+A', C_3+C_5), 67.74 (B+B', C_1+C_2). MS [*m/z* (% abundance)]: 184 (100), 271 (25), 538 (15). Elemental analysis calculated (%) for $C_{20}H_{16}N_2O_6Se_2 \cdot H_2O$: C: 43.18, H: 3.26, N: 5.04; found: C: 43.45, H: 3.52, N: 5.36.

*4.1.4. General procedure for the synthesis of compounds **1b–8b***

4-Aminophenyl selenocyanate (2 mmol) was dissolved in dry acetone (15 mL) and the corresponding anhydride (2 mmol) then added. The reaction was then stirred for a variable time of 12 h up to 48 h at room temperature. Reaction was quenched with water, compound was then filtered and purified by stirring or washing with solvents such as *n*-hexane and ethyl ether. The chemical shifts assignment in NMR spectroscopy for these compounds is exemplified in **Figure 11**.

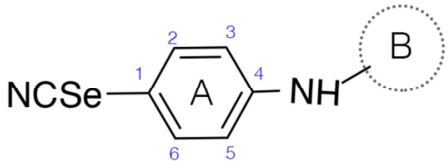

Figure 11. NMR assignation rules followed for series b.

*4.1.4.1. (2Z)-4-oxo-4-[(4-selenocyanatophenyl)amino]but-2-enoic acid (**1b**)*

From maleic anhydride. Conditions: 14 h at room temperature. The product was kept under stirring with water (25 mL) for 2 h, filtered and then washed with *n*-hexane (25 mL) and ethyl ether (25 mL). A yellow powder was obtained. Yield: 51.8%. Mp: 161–162ºC. IR (KBr) cm^{-1}:3299, 3196 (N-H), 2157 (CN), 1722 (C=O carboxylic acid), 1624 (C=O, amide). ^{1}H NMR (400 MHz, DMSO-d_6) δ: 12.96 (s, 1H, COOH), 10.58 (s, 1H, NH), 7.69 (bs, 4H, A, H_2+H_3+H_5+H_6), 6.47 (d, 1H, B, $J_{1\text{-}2}$= 12.0 Hz, H_1), 6.33 (d, 1H, B, $J_{2\text{-}1}$= 12.0 Hz, H_2). ^{13}C NMR (100 MHz, DMSO-d_6) δ: 167.37 (COOH), 164.02 (C=O), 140.42 (A, C_4), 135.24 (A, C_2+C_6), 132.04+130.75 (B, C_1+C_2), 121.16 (A, C_3+C_5), 117.57 (A, C_1), 105.77 (CN). ^{77}Se NMR (76 MHz, DMSO-d_6) δ: 322.45 (SeCN). MS [*m/z* (% abundance)]: 118 (100), 198 (25), 278 (10), 296 (7). Elemental

analysis calculated (%) for $C_{11}H_8N_2O_3Se$: C: 44.74, H: 2.73, N: 9.49; found: C: 44.35, H: 3.08, N: 9.10.

*4.1.4.2. 2-[(4-Selenocyanatophenyl)carbamoyl]benzoic acid (**2b**)*

From phthalic anhydride. Conditions: 14 h at room temperature. The product was kept under stirring with water (25 mL) for 2 h, filtered and then washed with *n*-hexane (25 mL) and ethyl ether (25 mL). A white powder was obtained. Yield: 89.5%. Mp: 162–164ºC. IR (KBr) cm^{-1}: 3317, 3122 (N-H), 2149 (CN), 1718 (C=O carboxylic acid), 1647 (C=O, amide). ^{1}H NMR (400 MHz, DMSO-d_6) δ: 13.14 (s, 1H, COOH), 10.60 (s, 1H, NH), 7.92 (d, 1H, B, $J_{3\text{-}4}$= 7.5 Hz, H_3), 7.78 (d, 2H, A, $J_{2\text{-}3}$=$J_{6\text{-}5}$= 8.3 Hz, H_2+H_6), 7.73–7.64 (m, 3H, A, H_3+H_5, B, H_4), 7.62–7.54 (m, 2H, B, H_5+H_6). ^{13}C NMR (100 MHz, DMSO-d_6) δ: 168.23 (COOH), 167.80 (C=O), 141.32+139.03 (A, C_4; B, C_1), 135.29 (A, C_2+C_6), 132.31 (B, C_5), 130.30+130.09+130.05 (B, C_2+C_3+C_4), 128.25 (B, C_6), 121.16 (A, C_1), 116.99 (A, C_3+C5), 105.91 (CN). MS [*m/z* (% abundance)]: 76 (50), 104 (55), 118 (100), 198 (20). Elemental analysis calculated (%) for $C_{15}H_{10}N_2O_3Se$: C: 52.19, H: 2.92, N: 8.11; found: C: 52.06, H: 3.24, N: 8.06.

*4.1.4.3. 4-Oxo-4-[(4-selenocyanatophenyl)amino]butanoic acid (**3b**)*

From succinic anhydride. Conditions: 24 h at room temperature. The product was kept under stirring with water (25 mL) for 2 h, filtered, then stirred with ethyl ether (100 mL) for 24 h and then filtered. A brown powder was obtained. Yield: 36.7%. Mp: 154–156ºC. IR (KBr) cm^{-1}: 3340 (NH), 2158 (CN), 1693 (C=O carboxylic acid), 1636 (C=O, amide). ^{1}H NMR (400 MHz, DMSO-d_6) δ: 12.18 (bs, 1H, COOH), 10.21 (s, 1H, NH), 7.66 (bs, 4H, A, H_2+H_6+H_3+H_5), 2.58 (d, 2H, A, $J_{2\text{-}1}$= 6.0 Hz, H_2), 2.54 (d, 2H, A, $J_{1\text{-}2}$= 6.0 Hz, H_1). ^{13}C NMR (100 MHz, DMSO-d_6) δ: 174.27 (COOH), 171.03 (C=O), 141.06

(A, C_4), 135.36 (A, C_2+C_6), 120.60 (A, C_3+C_5), 116.47 (A, C_1), 105.90 (CN), 31.54 (B, C_2), 29.10 (B, C_1). MS [m/z (% abundance)]: 101 (25), 118 (100), 198 (40), 298 (28). Elemental analysis calculated (%) for $C_{11}H_{10}N_2O_3Se_2 \cdot H_2O$: C: 41.92, H: 3.84, N: 8.89; found: C: 41.59, H: 3.58, N: 8.69.

*4.1.4.4. 3-[(4-Selenocyanatophenyl)carbamoyl]pyrazine-2-carboxylic acid (**4b**)*

From 2,3-pyrazinedicarboxylic anhydride. Conditions: 24 h at room temperature. The product was kept under stirring with water (25 mL) for 3 h, filtered, then stirred with ethyl ether (100 mL) for 24 h and then filtered. A yellow powder was obtained. Yield: 49.3%. Mp: 164–165ºC. IR (KBr) cm^{-1}: 3280 (NH), 2153 (CN), 1765 (C=O carboxylic acid), 1671 (C=O, amide). ^{1}H NMR (400 MHz, DMSO-d_6) δ: 13.82 (bs, 1H, COOH), 11.03 (s, 1H, NH), 8.92 (s, 2H, B, H_3+H_4), 7.87 (d, 2H, A, $J_{2\text{-}3}$=$J_{6\text{-}5}$= 8.6 Hz, H_2+H_6), 7.74 (d, 2H, A, $J_{3\text{-}2}$=$J_{5\text{-}6}$= 8.6 Hz, H_3+H_5). ^{13}C NMR (100 MHz, DMSO-d_6) δ: 167.05 (COOH), 163.64 (C=O), 146.99+146.75+146.15+145.49 (B, C_1+C_2+C_3+C_4), 140.49 (A, C_4), 135 (A, C_2+C_6), 122.19 (A, C_3+C_5), 118 (A, C_1), 106.37 (CN). MS [*m/z* (% abundance)]: 79 (100), 107 (95), 118 (30), 304 (75). Elemental analysis calculated (%) for $C_{13}H_8N_4O_3Se$: C: 44.97, H: 2.32, N: 16.14; found: C: 44.73, H: 2.72, N: 15.82.

*4.1.4.5. {2-Oxo-2-[(4-selenocyanatophenyl)amino]ethoxy}acetic acid (**5b**)*

From diglycolic anhydride. Conditions: 24 h at room temperature. The product was kept under stirring with water (25 mL) for 1 h, filtered and then washed with ethyl ether (2 × 25 mL). A white powder was obtained. Yield: 51.1%. Mp: 141–142ºC. IR (KBr) cm^{-1}: 3305 (NH), 2151 (CN), 1716 (C=O carboxylic acid), 1660 (C=O, amide). ^{1}H NMR (400 MHz, DMSO-d_6) δ: 12.91 (bs, 1H, COOH), 10.14 (s, 1H, NH), 7.74 (d, 2H, A, $J_{2\text{-}3}$=$J_{6\text{-}5}$= 8.8 Hz, H_2+H_6), 7.68 (d, 2H, A, $J_{3\text{-}2}$=$J_{5\text{-}6}$= 8.8 Hz, H_3+H_5), 4.21 (s, 2H, B, H_1), 4.20

(s, 2H, B, H_2). ^{13}C NMR (100 MHz, DMSO-d_6) δ: 172.25 (COOH), 168.78 (C=O), 140.14 (A, C_4), 135.27 (A, C_2+C_6), 121.30 (A, C_3+C_5), 117.43 (A, C_1), 105.92 (CN), 70.83 (B, C_1), 68.51 (B, C_2). MS [*m/z* (% abundance)]: 118 (85), 198 (40), 211 (30), 314 (100). Elemental analysis calculated (%) for $C_{11}H_{10}N_2O_4Se$: C: 42.19, H: 3.22, N: 8.95; found: C: 41.92, H: 3.53, N: 8.82.

*4.1.4.6. 2'-[(4-Selenocyanatophenyl)carbamoyl]-[1,1'-biphenyl]-2-carboxylic acid (**6b**)*

From diphenic anhydride. Conditions: 48 h at room temperature. The product was kept under stirring with water (25 mL) for 3 h, filtered and then washed with ethyl ether (2 × 25 mL). A white powder was obtained. Yield: 21.8%. Mp: 146–147ºC. IR (KBr) cm^{-1}: 3296 (NH), 2153 (CN), 1726 (C=O, carboxylic acid), 1631 (C=O, amide). ^{1}H NMR (400 MHz, DMSO-d_6) δ: 12.80 (bs, 1H, COOH), 10.24 (s, 1H, NH), 7.83 (d, 1H, B, $J_{9\text{-}10}$=7.6 Hz, H_9), 7.67–7.58 (m, 3H, B, H_2+H_5+H_{12}), 7.58–7.48 (m, 5H, A, H_2+H_3+H_5+H_6, B, H_{11}),7.41 (t, 1H, B, $J_{4\text{-}3}$=$J_{4\text{-}5}$= 7.4 Hz, H_4), 7.24 (t, 2H, B, $J_{3\text{-}2}$=$J_{3\text{-}4}$=$J_{10\text{-}9}$=$J_{10\text{-}11}$= 5.9 Hz, H_3+H_{10}). ^{13}C NMR (100 MHz, DMSO-d_6) δ: 169.20 (COOH), 167.55 (C=O), 141.41 (A, C_4), 140.79+140.76 (B, C_6+C_7), 136.14 (B, C_8), 135.19 (A, C_2+C_6), 131.67 (B, C_1), 131.42+131.07+130.45+130.11+129.84 (B, C_2+C_3+C_4+C_9+C_{11}), 127.88+127.78+127.55 (B, C_5+C_{10}+C_{12}), 121.06 (A, C_3+C_5), 117.14 (A, C_1), 105.89 (CN). MS [*m/z* (% abundance)]: 152 (70), 181 (100), 225 (30), 422 (10). Elemental analysis calculated (%) for $C_{21}H_{14}N_2O_3Se \cdot 2H_2O$: C: 55.15, H: 3.97, N: 6.13; found: C: 55.39, H: 3.59, N: 6.22.

*4.1.4.7. 2-[(4-Selenocyanatophenyl)carbamoyl]cyclohexanecarboxylic acid (**7b**)*

From cis-1,2-cyclohexanecarboxylic anhydride. Conditions: 24 h at room temperature. The product was kept under stirring with water (25 mL) for 2 h, filtered and then

washed with ethyl ether (2 × 25 mL). A white powder was obtained. Yield: 47.0%. Mp: 150–151ºC. IR (KBr) cm^{-1}: 3335 (NH), 2152 (CN), 1702 (C=O, carboxilic acid), 1677 (C=O, amide) ^{1}H NMR (400 MHz, DMSO-d_6) δ: 11.99 (bs, 1H, COOH), 9.95 (s, 1H, NH), 7.66 (d, 2H, A, $J_{2\text{-}3}$=$J_{6\text{-}5}$= 8.5 Hz, H_2+H_6), 7.62 (d, 2H, A, $J_{3\text{-}2}$=$J_{5\text{-}6}$= 8.5 Hz, H_3+H_5), 2.94 (d, 1H, B, $J_{1\text{-Hchex}}$= 4.0 Hz, H_1), 2.60 (d, 1H, B, $J_{\text{chex-1}}$ = 4.0 Hz, H_{chex}), 2.09 (d, 1H, B, J= 9.7 Hz, H_{chex}), 1.99 (d, 1H, B, J= 8.8 Hz, H_{chex}), 1.82–1.57 (m, 3H, B, 3Hchex), 1.48–1.24 (m, 3H, B, 3Hchex). ^{13}C NMR (100 MHz, DMSO-d_6) δ: 175.55 (COOH), 173.56 (C=O), 141.39 (A, C_4), 135.24 (A, C_2+C_6), 120.76 (A, C_3+C_5), 116.18 (A, C_1), 105.87 (CN), 43.05+42.42 (B, C_1+C_2), 28.06+25.64+24.44+22.78 (B, C_3+C_4+C_5+C_6). MS [*m/z* (% abundance)]: 67 (90), 81 (93), 118 (100), 198 (60), 334 (100). Elemental analysis calculated (%) for $C_{15}H_{16}N_2O_3Se \cdot H_2O$: C: 48.79, H: 4.91, N: 7.59; found: C: 48.56, H: 4.72, N: 7.66.

*4.1.4.8. 3-[(4-Selenocyanatophenyl)carbamoyl]-7-oxabicyclo[2.2.1]hept-5-ene-2-carboxylic acid (**8b**)*

From 3,6-epoxy-1,2,3,6-tetrahydrophthalic anhydride obtained by the classic procedure described for a Diels-Alder reaction using furan and maleic anhydride as reagents to yield the Diels-Alder adduct. Conditions: 24 h at room temperature. The product was kept under stirring with water (25 mL) for 4 h, filtered and then washed with ethyl ether (2 × 25 mL). A light-yellow powder was obtained. Yield: 20.3%. Mp: 155–156ºC. IR (KBr) cm^{-1}: 3267 (NH), 1711 (C=O carboxylic acid), 1689 (C=O, amide). ^{1}H NMR (400 MHz, DMSO-d_6) δ: 12.19 (s, 1H, COOH), 10.03 (s, 1H, NH), 7.65 (d, 2H, A, $J_{2\text{-}3}$=$J_{6\text{-}5}$= 9.0 Hz, H_2+H_6), 7.62 (d, 2H, A, $J_{3\text{-}2}$=$J_{5\text{-}6}$= 9.0 Hz, H_3+H_5), 6.50 (s, 2H, B, H_3+H_5), 5.14 (s, 1H, B, H_5), 5.06 (s, 1H, B, H_2), 2.82 (d, 1H, B, $J_{1\text{-}6}$= 9.1 Hz, H_1), 2.71 (d, 1H, B, $J_{6\text{-}1}$= 9.1 Hz, H_6). ^{13}C NMR (100 MHz, DMSO-d_6) δ: 173.08 (COOH),

170.48 (C=O), 141.07 (A, C_4), 137.49+137.08 (B, C_4+C_5), 135.29 (A, C_2+C_6), 120.79 (A, C_3+C_5), 116.51 (A, C_1), 105.93 (CN), 80.82+79.61 (B, C_3+C_6), 47.96+47.36 (B, C_1+C_2). ^{77}Se NMR (76 MHz, DMSO-d_6) δ: 320.95 (SeCN). MS [*m/z* (% abundance)]: 68 (100), 118 (100), 198 (25), 278 (10). Elemental analysis calculated (%) for $C_{15}H_{12}N_2O_4Se \cdot ½\ H_2O$: C: 48.35, H: 3.49, N: 7.52; found: C: 48.30, H: 3.70, N: 7.53.

4.2. Biological evaluation

4.2.1. Cell cultures

Cell lines were purchased from the American Type Culture Collection (ATCC). PC-3, HTB-54, HT-29, MOLT-4, CCRF-CEM, K-562 and MCF-7 cell lines were grown in RPMI 1640 medium (Gibco) supplemented with 10% fetal bovine serum (FBS; Gibco), 100 units/mL penicillin and 100 mg/mL streptomycin (Gibco). BEAS-2B cell line (normal epithelial lung) was cultured in DMEM (Gibco), 10% FBS, 100 units/mL penicillin and 100 μg/mL streptomycin. 184B5 cells were grown in DMEM/F12 medium supplemented with 5% FBS, 1× ITS (Lonza), 100 nM hydrocortisone (Aldich), 2 mM sodium pyruvate (Lonza), 20 ng/mL EGF (Sigma- Aldrich), 0.3 nM *trans*-retinoic acid (Sigma-Aldrich), 100 units/mL penicillin and 100 mg/mL streptomycin. Cells were maintained at 37ºC and 5% CO_2.

4.2.2. Cytotoxic and antiproliferative activities

Cell viability was determined using the MTT 3-(4,5-dimethylthiazol-2-yl)-2,5-diphenyl-tetrazolium bromide) method at 10 and 100 μM to perform the screening. In order to build full dose-response curves five different doses ranging from 0.01 to 100 μM, for some compounds lower doses where needed in order to reach 50% cell growth. Depending on cell size, 8,000 to 40,000 cells were seeded per well in 96-well plates and incubated overnight. Then treated with the compounds for 48 h, cells were then

incubated with 50 μL of MTT (2 mg/mL stock) for 4 h, medium was removed by aspiration and formazan crystals dissolved in 150 μL of DMSO. The absorbance was measured at 550 nm in a microplate reader (Sunrise reader, Tecan). At least three independent experiments performed in quadruplicate were analysed. Results are expressed as GI_{50}, the concentration that reduces by 50% the growth of treated cells with respect to untreated controls, TGI, the concentration that completely inhibits cell growth, and LC_{50}, the concentration that kills 50% of the cells.

4.2.3. Evaluation of cell cycle progression and cell death

A fixed population of MCF-7 cells per flask were seeded in 25 cm^2 flasks then incubated overnight. Cultures were treated with the corresponding amount of compounds **10a**, **8b**, DMSO (control) or 6 μM camptothecin (positive control). Seeded population was dependent on studied time point: 3×10^6 cells/flask for 24 h or shorter treatment, 2×10^6 cells/flasks for 48 h treatment and finally 1×10^6 cells/flask for 72 h experiments. Apo-Direct kit (BD Pharmigen) was used to determine cell cycle distribution and cell death percentage. Cells were fixed in a 1% paraformaldehyde solution in PBS for 30–40 min at 0ºC, washed with PBS twice and incubated for 30 min with 70% ethanol on ice. Staining was performed following manufacturer's protocol and samples were analysed by flow cytometry using a Counter Epics XL cytometer (Beckman Counter).

Inhibition assays cells were pre-treated with 50 μM of the pan-caspase inhibitor Z-VAD-FMK (BD Pharmigen) or 100 nM of the autophagy inhibitor wortmannin (Santa Cruz) for 1 h or 10 μM of chloroquine (Sigma Aldrich). The cells were treated with 80 μM of **8b** or **10a**, DMSO was added to the control cells. Samples were processed

following the same methodology stated above. At least three independent experiments were performed in duplicate.

4.2.4. Statistical analysis

Statistical data represent the mean ± SEM of at least three independent experiments performed in duplicate. Mann-Whitney U-test was used to stablish statistical significance of differences between control and treatment groups. GraphPad Prism version 7 was used, significant differences were considered at $p < 0.05$.

4.2.5. Protein analysis

Proteins were detected by western blot. Specific antibodies for LC3B, Beclin-1 (D40C5), SQSTM1/p62, AMPK, JNK, pAKT (Se473) and the PI3K catalytic subunit p110α were obtained from Cell Signalling. Anti-actin (H-300) was from Santa Cruz Biotechnology. Anti-rabbit IgG conjugated with peroxidase (Cell Signaling) was used as secondary antibody.

Acknowledgments

The research leading to these results has received funding from "la Caixa" Banking Foundation. P. Garnica wishes to express his gratitude to the Asociación de Amigos de la Universidad de Navarra for the pre-doctoral fellowship. Furthermore, the authors wish to express their gratitude to the Plan de Investigación de la Universidad de Navarra, PIUNA (Ref 2014–26) as well as Caixa Foundation-UNED for financial support for the project.

References

[1] R.L. Siegel, K.D. Miller, A.A.-O.h.o.o. Jemal, Cancer statistics, 2018, Ca-Cancer J. Clin. 68 (2018) 7-30. https://doi.org/10.3322/caac.21442.

[2] P. Bhat, J. Kriel, B. Shubha Priya, Basappa, N.S. Shivananju, B. Loos, Modulating autophagy in cancer therapy: Advancements and challenges for cancer cell death sensitization, Biochem. Pharmacol. 147 (2018) 170-182. https://doi.org/10.1016/j.bcp.2017.11.021.

[3] C. Bi, N. Zhang, P. Yang, C. Ye, Y. Wang, T. Fan, R. Shao, H. Deng, D. Song, Synthesis, biological evaluation, and autophagy mechanism of 12N-substituted sophoridinamines as novel anticancer agents, ACS Med. Chem. Lett. 8 (2017) 245-250. https://doi.org/10.1021/acsmedchemlett.6b00466.

[4] Y.Y. Zhou, Y. Li, W.Q. Jiang, L.F. Zhou, MAPK/JNK signalling: A potential autophagy regulation pathway, Biosci. Rep. 35 (2015). https://doi.org/10.1042/BSR20140141.

[5] D.D. Li, L.L. Wang, R. Deng, J. Tang, Y. Shen, J.F. Guo, Y. Wang, L.P. Xia, et al., The pivotal role of c-JUN NH2-terminal kinase-mediated Beclin 1 expression during anticancer agents-induced autophagy in cancer cells, Oncogene 28 (2009) 886-898. https://doi.org/10.1038/onc.2008.441.

[6] R.C. Russell, H.X. Yuan, K.L. Guan, Autophagy regulation by nutrient signaling, Cell Res. 24 (2014) 42-57. https://doi.org/10.1038/cr.2013.166.

[7] K. Inoki, T. Zhu, K.L. Guan, TSC2 mediates cellular energy response to control cell growth and survival, Cell 115 (2003) 577-590. https://doi.org/https://doi.org/10.1016/S0092-8674(03)00929-2.

[8] S. Kanno, S. Yomogida, A. Tomizawa, H. Yamazaki, K. Ukai, R.E.P. Mangindaan, M. Namikoshi, M. Ishikawa, Papuamine causes autophagy following the reduction of

cell survival through mitochondrial damage and JNK activation in MCF-7 human breast cancer cells, Int. J. Oncol. 43 (2013) 1413-1419. https://doi.org/10.3892/ijo.2013.2093.

[9] Z.L. Sun, J.L. Dong, J. Wu, Juglanin induces apoptosis and autophagy in human breast cancer progression via ROS/JNK promotion, Biomed. Pharmacother. 85 (2017) 303-312. https://doi.org/10.1016/j.biopha.2016.11.030.

[10] S. Kang, J.E. Kim, N.R. Song, S.K. Jung, M.H. Lee, J.S. Park, M.H. Yeom, A.M. Bode, Z. Dong, K.W. Lee, The ginsenoside 20-o-beta-d-glucopyranosyl-20(S)-protopanaxadiol induces autophagy and apoptosis in human melanoma via AMPK/JNK phosphorylation, PLoS One 9 (2014) e104305. https://doi.org/10.1371/journal.pone.0104305.

[11] A. Puissant, G. Robert, N. Fenouille, F. Luciano, J.P. Cassuto, S. Raynaud, P. Auberger, Resveratrol promotes autophagic cell death in chronic myelogenous leukemia cells via JNK-mediated p62/SQSTM1 expression and ampk activation, Cancer Res. 70 (2010) 1042-1052. https://doi.org/10.1158/0008-5472.CAN-09-3537.

[12] Q. Miao, J. Xu, A. Lin, X. Wu, L. Wu, W. Xie, Recent advances for the synthesis of selenium-containing small molecules as potent antitumor agents, Curr. Med. Chem. 25 (2017) 2009-2033. https://doi.org/10.2174/0929867325666171129220544.

[13] D. Bartolini, L. Sancineto, A. Fabro de Bem, K.D. Tew, C. Santi, R. Radi, P. Toquato, F. Galli, Selenocompounds in cancer therapy: An overview, Adv. Cancer. Res. 136 (2017) 259-302. https://doi.org/10.1016/bs.acr.2017.07.007.

[14] Y. Yang, H. Luo, K. Hui, Y. Ci, K. Shi, G. Chen, L. Shi, C. Xu, Selenite-induced autophagy antagonizes apoptosis in colorectal cancer cells *in vitro* and *in vivo*, Oncol. Rep. 35 (2016) 1255-1264. https://doi.org/10.3892/or.2015.4484.

[15] J.C. Wu, F.Z. Wang, M.L. Tsai, C.Y. Lo, V. Badmaev, C.T. Ho, Y.J. Wang, M.H. Pan, Se-allylselenocysteine induces autophagy by modulating the AMPK/mTOR

signaling pathway and epigenetic regulation of PCDH17 in human colorectal adenocarcinoma cells, Mol. Nutr. Food.Res. 59 (2015) 2511-2522. https://doi.org/10.1002/mnfr.201500373.

[16] Y.F. Zou, P.Y. Niu, J. Yang, J. Yuan, T.C. Wu, X.M. Chen, The JNK signaling pathway is involved in sodium-selenite-induced apoptosis mediated by reactive oxygen in HEPG2 cells, Cancer Biol. Ther. 7 (2008) 689-696. https://doi.org/10.4161/cbt.7.5.5688.

[17] K. Wang, X.T. Fu, Y. Li, Y.J. Hou, M.F. Yang, J.Y. Sun, S.Y. Yi, C.D. Fan, et al., Induction of S-phase arrest in human glioma cells by selenocysteine, a natural selenium-containing agent via triggering reactive oxygen species-mediated DNA damage and modulating MAPKs and AKT pathways, Neurochem. Res. 41 (2016) 1439-1447. https://doi.org/10.1007/s11064-016-1854-8.

[18] P. Chakraborty, S.S. Roy, A. Basu, S. Bhattacharya, Sensitization of cancer cells to cyclophosphamide therapy by an organoselenium compound through ROS-mediated apoptosis, Biomed. Pharmacother. 84 (2016) 1992-1999. https://doi.org/10.1016/j.biopha.2016.11.006.

[19] C. Kim, J. Lee, M.-S. Park, Synthesis of new diorganodiselenides from organic halides: Their antiproliferative effects against human breast cancer MCF-7 cells, Arch. Pharm. Res. 38 (2014) 659-665. https://doi.org/10.1007/s12272-014-0407-4.

[20] D. Plano, Y. Baquedano, E. Ibanez, I. Jimenez, J.A. Palop, J.E. Spallholz, C. Sanmartin, Antioxidant-prooxidant properties of a new organoselenium compound library, Molecules 15 (2010) 7292-7312. https://doi.org/10.3390/molecules15107292.

[21] P. Garnica, I. Encio, D. Plano, J.A. Palop, C. Sanmartin, Combined acylselenourea-diselenide structures: New potent and selective antitumoral agents as

autophagy activators, ACS Med. Chem. Lett. 9 (2018) 306-311. https://doi.org/10.1021/acsmedchemlett.7b00482.

[22] V. Bala, S. Rao, P. Li, S. Wang, C.A. Prestidge, Lipophilic prodrugs of SN38: Synthesis and in vitro characterization toward oral chemotherapy, Mol. Pharm. 13 (2015) 287-294. https://doi.org/10.1021/acs.molpharmaceut.5b00785.

[23] M. Majekova, J. Ballekova, M. Prnova, M. Stefek, Structure optimization of tetrahydropyridoindole-based aldose reductase inhibitors improved their efficacy and selectivity, Bioorg. Med. Chem. 25 (2017) 6353-6360. https://doi.org/10.1016/j.bmc.2017.10.005.

[24] G. Huang, A. Drakopoulos, M. Saedtler, H. Zou, L. Meinel, J. Heilmann, M. Decker, Cytotoxic properties of the alkaloid rutaecarpine and its oligocyclic derivatives and chemical modifications to enhance water-solubility, Bioorg. Med. Chem. Lett. 27 (2017) 4937-4941. https://doi.org/10.1016/j.bmcl.2017.08.045.

[25] V. Gota, J.S. Goda, K. Doshi, A. Patil, S. Sunderajan, K. Kumar, M. Varne, A. Kunwar, V.K. Jain, I. Priyadarshini, Biodistribution and pharmacokinetic study of 3,3′ diseleno dipropionic acid (DSEPA), a synthetic radioprotector, in mice, Eur. J. Drug Metabol. 41 (2015) 839-844. https://doi.org/10.1007/s13318-015-0301-6.

[26] K.E. Machado, K.N. Oliveira, L. Santos-Bubniak, M.A. Licinio, R.J. Nunes, M.C. Santos-Silva, Evaluation of apoptotic effect of cyclic imide derivatives on murine B16F10 melanoma cells, Bioorg. Med. Chem. 19 (2011) 6285-6291. https://doi.org/10.1016/j.bmc.2011.09.008.

[27] D. Rosolen, I.F. Kretzer, E. Winter, V.F. Noldin, I.A. Rodrigues do Carmo, F.B. Filippin-Monteiro, V. Cechinel-Filho, T.B. Creczynski-Pasa, N-phenylmaleimides affect adipogenesis and present antitumor activity through reduction of FASN

expression, Chem. Biol. Interact. 258 (2016) 10-20. https://doi.org/10.1016/j.cbi.2016.08.005.

[28] B. Romano, D. Plano, I. Encio, J.A. Palop, C. Sanmartin, In vitro radical scavenging and cytotoxic activities of novel hybrid selenocarbamates, Bioorg. Med. Chem. 23 (2015) 1716-1727. https://doi.org/10.1016/j.bmc.2015.02.048.

[29] E. Dominguez-Alvarez, D. Plano, M. Font, A. Calvo, C. Prior, C. Jacob, J.A. Palop, C. Sanmartin, Synthesis and antiproliferative activity of novel selenoester derivatives, Eur. J. Med. Chem. 73 (2014) 153-166. https://doi.org/10.1016/j.ejmech.2013.11.034.

[30] V. Alcolea, D. Plano, D.N. Karelia, J.A. Palop, S. Amin, C. Sanmartin, A.K. Sharma, Novel seleno- and thio-urea derivatives with potent in vitro activities against several cancer cell lines, Eur. J. Med. Chem. 113 (2016) 134-144. https://doi.org/10.1016/j.ejmech.2016.02.042.

[31] V. Alcolea, D. Plano, I. Encio, J.A. Palop, A.K. Sharma, C. Sanmartin, Chalcogen containing heterocyclic scaffolds: New hybrids with antitumoral activity, Eur. J. Med. Chem. 123 (2016) 407-418. https://doi.org/10.1016/j.ejmech.2016.07.042.

[32] N. Diaz-Argelich, I. Encio, D. Plano, A.P. Fernandes, J.A. Palop, C. Sanmartin, Novel methylselenoesters as antiproliferative agents, Molecules 22 (2017) 1288. https://doi.org/10.3390/molecules22081288.

[33] M. Diaz, R. Gonzalez, D. Plano, J.A. Palop, C. Sanmartin, I. Encio, A diphenyldiselenide derivative induces autophagy via JNK in HTB-54 lung cancer cells, J. Cell. Mol. Med. 22 (2018) 289-301. https://doi.org/10.1111/jcmm.13318.

[34] Z. Han, B. Li, J. Wang, X. Zhang, Z. Li, L. Dai, M. Cao, J. Jiang, Norcantharidin inhibits SK-N-SH neuroblastoma cell growth by induction of autophagy and apoptosis,

Technol. Cancer Res. Treat. 16 (2016) 33-44. https://doi.org/10.1177/1533034615624583.

[35] M. Dalvai, K. Bystricky, Cell cycle and anti-estrogen effects synergize to regulate cell proliferation and ER target gene expression, PLoS One 5 (2010) e11011. https://doi.org/10.1371/journal.pone.0011011.

[36] H. Hamouchene, V.M. Arlt, I. Giddings, D.H. Phillips, Influence of cell cycle on responses of MCF-7 cells to benzo[a]pyrene, BMC Genomics 12 (2011) 333. https://doi.org/10.1186/1471-2164-12-333.

[37] M. Hamada, H. Kameyama, S. Iwai, Y. Yura, Induction of autophagy by sphingosine kinase 1 inhibitor PF-543 in head and neck squamous cell carcinoma cells, Cell Death Discov. 3 (2017) 17047. https://doi.org/10.1038/cddiscovery.2017.47.

[38] P. Fabbrizio, S. Amadio, S. Apolloni, C. Volonte, P2x7 receptor activation modulates autophagy in SOD1-G93A mouse microglia, Front. Cell. Neurosci. 11 (2017) 249. https://doi.org/10.3389/fncel.2017.00249.

[39] H.J. Jung, J.H. Kang, S. Choi, Y.K. Son, K.R. Lee, J.K. Seong, S.Y. Kim, S.H. Oh, Pharbitis nil (PN) induces apoptosis and autophagy in lung cancer cells and autophagy inhibition enhances PN-induced apoptosis, J. Ethnopharmacol. 208 (2017) 253-263. https://doi.org/10.1016/j.jep.2017.07.020.

[40] D.J. Klionsky, K. Abdelmohsen, A. Abe, M.J. Abedin, H. Abeliovich, A. Acevedo Arozena, H. Adachi, C.M. Adams, et al., Guidelines for the use and interpretation of assays for monitoring autophagy (3rd edition), Autophagy 12 (2016) 1-222. https://doi.org/10.1080/15548627.2015.1100356.

[41] K. Wang, C. Zhang, J. Bao, X. Jia, Y. Liang, X. Wang, M. Chen, H. Su, et al., Synergistic chemopreventive effects of curcumin and berberine on human breast cancer

cells through induction of apoptosis and autophagic cell death, Sci. Rep. 6 (2016) 26064. https://doi.org/10.1038/srep26064.

[42] S. Faes, O. Dormond, PI3K and AKT: Unfaithful partners in cancer, Int. J. Mol. Sci. 16 (2015) 21138-21152. https://doi.org/10.3390/ijms160921138.

[43] X. Wu, S. Renuse, N.A. Sahasrabuddhe, M.S. Zahari, R. Chaerkady, M.S. Kim, R.S. Nirujogi, M. Mohseni, et al., Activation of diverse signalling pathways by oncogenic PIK3CA mutations, Nat. Commun. 5 (2014) 4961. https://doi.org/10.1038/ncomms5961.

[44] A. Guerrero-Zotano, I.A. Mayer, C.L. Arteaga, PI3K/AKT/mTOR: Role in breast cancer progression, drug resistance, and treatment, Cancer Metastasis Rev. 35 (2016) 515-524. https://doi.org/10.1007/s10555-016-9637-x.

[45] X.L. Xu, J. Sun, R.L. Song, M.E. Doscas, A.J. Williamson, J.S. Zhou, J. Sun, X.N. Jiao, X.F. Liu, Y. Li, Inhibition of p70 S6 kinase (S6K1) activity by A77 1726, the active metabolite of leflunomide, induces autophagy through TAK1-mediated AMPK and JNK activation, Oncotarget 8 (2017) 30438-30454. https://doi.org/10.18632/oncotarget.16737.

[46] J.N. Hutchinson, J. Jin, R.D. Cardiff, J.R. Woodgett, W.J. Muller, Activation of AKT-1 (PKB-alpha) can accelerate ERBB-2-mediated mammary tumorigenesis but suppresses tumor invasion, Cancer Res. 64 (2004) 3171-3178. https://doi.org/10.1158/0008-5472.

[47] S. Brolih, S.K. Parks, V. Vial, J. Durivault, L. Mostosi, J. Pouyssegur, G. Pages, V. Picco, AKT1 restricts the invasive capacity of head and neck carcinoma cells harboring a constitutively active PI3 kinase activity, BMC Cancer 18 (2018) 249. https://doi.org/10.1186/s12885-018-4169-0.

Highlights

- 17 selenium derivates related to selenocyanates and diselenides were synthesized.
- **8b** and **10a** were highly selective towards MCF-7 cells.
- **8b** and **10a** induce cell cycle arrest in S phase.
- **8b** and **10a** modulate AMPK and JNK signaling pathway.
- **8b** and **10a** induce autophagy-mediated cell death.

Organoseleno cytostatic derivatives: autophagic cell death with AMPK and JNK activation.

Pablo Garnica [1,2], Ignacio Encío [2,3], Daniel Plano [1,2], Juan A. Palop [1,2], Carmen Sanmartín [1,2]*

[1] Universidad de Navarra, Facultad de Farmacia y Nutrición, Departamento de Tecnología y Química Farmacéuticas. Campus Universitario, 31080, Pamplona, España
[2] Instituto de Investigación Sanitaria de Navarra (IdiSNA), Irunlarrea 3, E-31008 Pamplona, Spain
[3] Department of Health Sciences, Public University of Navarra, Avda. Barañain s/n, E-31008 Pamplona, Spain

* Prof. Carmen Sanmartín

Department of Pharmaceutical Technology and Chemistry

University of Navarra

Irunlarrea, 1, E-31008 Pamplona

SPAIN

+34 948 425 600 (Telephone)

+34 948 425 649 (Fax)

e-mail: sanmartin@unav.es

Abstract

Selenocyanates and diselenides are potential antitumor agents. Here we report two series of selenium derivatives related to selenocyanates and diselenides containing carboxylic, amide and imide moieties. These compounds were screened for their potency and selectivity against seven tumor cell lines and two non-malignant cell lines. Results showed that MCF-7 cells were especially sensitive to the treatment, with seven compounds presenting GI_{50} values below 10 μM. Notably, the carboxylic selenocyanate **8b** and the cyclic imide **10a** also displayed high selectivity for tumor cells. Treatment of MCF-7 cells with these compounds resulted in cell cycle arrest at S phase, increased levels of pJNK and pAMPK and caspase independent cell death. Autophagy inhibitors wortmannin and chloroquine partially prevented **8b** and **10a** induced cell death. Consistent with autophagy, increased Beclin1 and LC3-IIB and reduced SQSTM1/p62 levels were detected. Our results point to **8b** and **10a** as autophagic cell death inducers.

Keywords: Autophagy, cancer, cyclic imide, diselenide, selenocyanate.

1. Introduction

Despite recent advances in development of anticancer agents, this illness remains a leading cause of disease-related death worldwide [1]. Due to their effect on several survival or death signaling pathways that may decide the fate of cancer cells [2, 3], therapies based on autophagy targeted agents are now in the focus of a wide range of researchers. Among the signaling pathways implicated in these processes, JNK activation has been proven to participate in multiple autophagic events such as Beclin1 expression and autophagic-mediated cell death [4, 5]. Energetic stress has also been described to be a trigger for autophagy [6]; in this context, AMPK has been proven to have an essential role promoting autophagy by inhibiting the mTORs regulatory cascade [7]. The phosphorylation of AMPK and JNK in autophagy-mediated cell death has been previously described in breast adenocarcinoma [8, 9] and several other cancer types such as myeloma [10] and leukemia [11].

During the past decade, extensive studies of selenium compounds have demonstrated their antitumor and chemopreventive activities in a vast array of experimental models [12]. These derivatives interfere with the redox homeostasis and signaling of cancer cells. The mechanism by which they cause their effect include alterations in cell cycle checkpoints, proliferation, senescence, and death pathways [13]. In addition, some selenium derivatives such as selenite, selenocysteine and *Se*-allylselenocysteine play an effective role in cancer treatment as autophagy inducers and modulators of the JNK signaling pathway [14-17].

Many chemical entities containing selenium, with potent antitumor activity, have been explored by the scientific community. Among them, selenocyanate [18] and diselenide [19] moieties have been highlighted due to their interesting antitumor properties. In this line of investigation two effective derivatives, the diselenide analog bis(4-

aminophenyl)diselenide (**0a**) and the corresponding selenocyanate (**0b**), were recently identified in our laboratory [20]. In order to obtain a second generation of selenium structures with improved activity, selectivity and water solubility these compounds have been used as a starting point to continue with their modulation [21]. It is remarkable that one of the limitations of the selenium derivatives is their poor water solubility which is detrimental for their bioavailability and drug development. To obtain compounds with improved pharmacokinetic properties, modifications in the hydrophobic scaffold that improve water solubility are usually assayed. As an example of this strategy, introduction of a hydroxyl group in the phenyl ring of the natural product camptothecin has been shown to counteract efficiently this drawback [22]. Thus, a useful option when using this approach is to incorporate polar functional groups, such as acidic or basic groups. These fragments enable the possibility of salt formation and therefore might enhance water solubility [23, 24]. In this study, substantial efforts had been directed towards finding different chemical scaffolds that, while maintaining the cytotoxic activity, should increase the hydrophilicity further contributing to the solubility optimization. Among the structural features incorporated, we surmised that the introduction of the carboxylic core could be a logical approach for improving its aqueous solubility. This moiety is present in widely described organoselenium compounds such as 3,3'-diselenodipropionic acid [25]. In addition, the dicarboxylic acids are of special importance because of their versatility in the preparation of the corresponding cyclic imide homologs which are widely described in the literature as potential antitumor agents [26, 27].

Taking into consideration the facts stated above and our previous work in the field of new selenium compounds as antitumor agents [21, 28-33], the present study aimed to synthesize selenocyanates and diselenides containing carboxylic, amide and imide

moieties. The general outline of this series of compounds is presented in **Figure 1**. Variations were made in the group linked to the carboxy feature through selection of different cyclic symmetric anhydrides commercially available such as maleic, succinic, phthalic... Finally, with the objective of widening the structural variations, a new anhydride was synthesized through the Diels-Alder cycloaddition. The rationality behind this proposal is the synthesis of a structural analog of norcantharidin, a well-known active antitumor autophagy inducer [34].

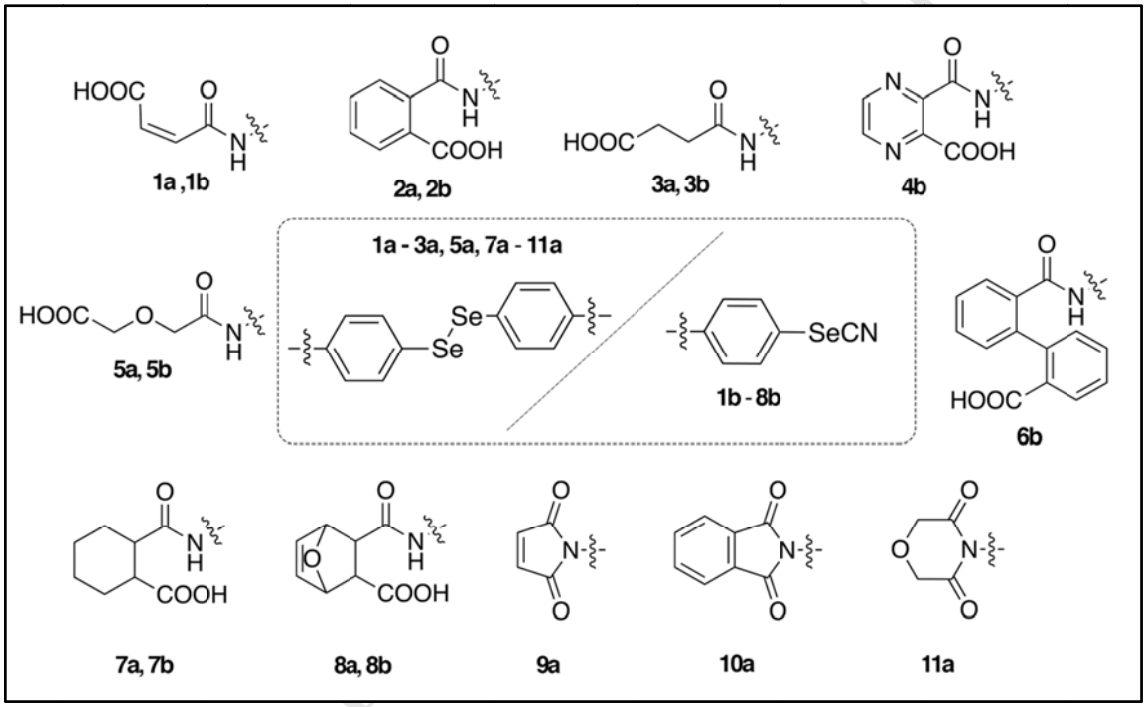

Figure 1. Structures of novel selenium containing compounds.

2. Results and discussion

2.1. Chemistry

The seventeen compounds synthesized and presented in this work can be categorized into two different subseries according to their selenium moiety:

- Diselenide derivatives containing carboxylic and amide or imide moieties (**1a-3a**, **5a**, **7a-11a**).
- Selenocyanate derivatives containing carboxylic and amide moieties (**1b-8b)**.

The resulting compounds were numbered according to the corresponding anhydride used as starting material.

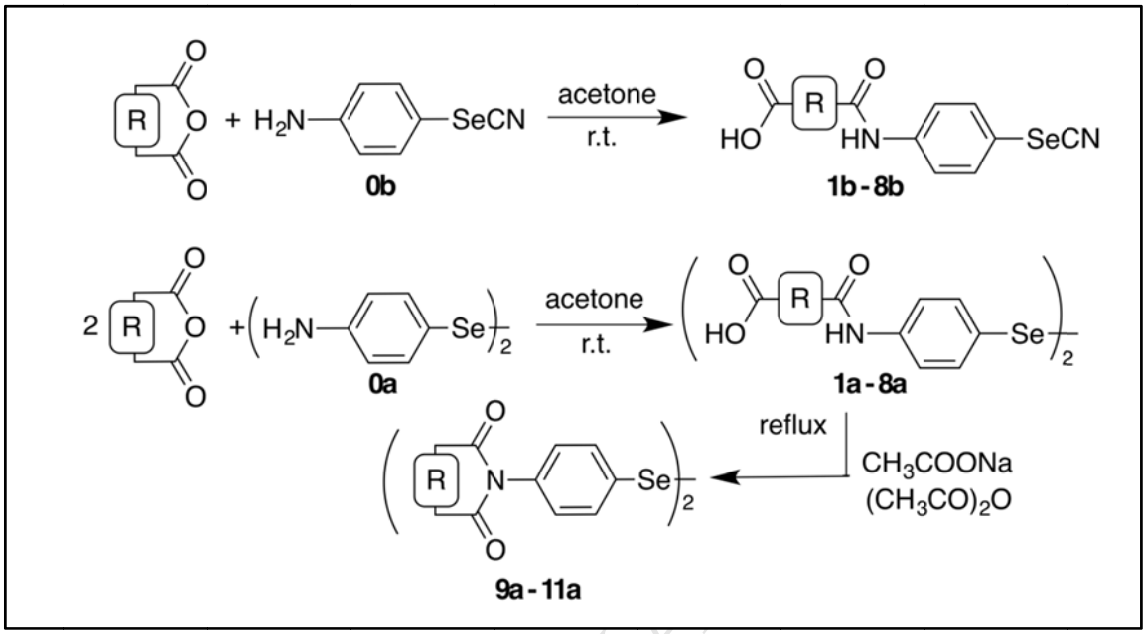

Figure 2. General procedure of synthesis.

Derivatives were synthesized following the synthetic path depicted in **Figure 2**. The corresponding anhydrides were reacted with either bis(4-aminophenyl)diselenide (**0a**) or 4-aminophenylselenocyanate (**0b**) in acetone at room temperature for 8 h up to 24 h. The formed precipitate was filtered and washed with *n*-hexane or ethyl ether to yield the final compounds. The mechanism proposed for this reaction is a nucleophilic acyl substitution illustrated in **Figure 3A**. Moreover, all our attempts to generate derivatives **4a** and **6a** were unsuccessful since the reaction of the corresponding anhydrides with **0a** in different conditions (temperature, solvents and catalyst) failed to yield the desired compound. Unfortunately, the alternative strategy of reducing their selenocyanate analogs (**4b** and **6b**) to obtain derivatives **4a** and **6a** under different conditions only resulted in the degradation of the start-up derivatives. To obtain the cyclic imides (**9a-11a**), the corresponding amidic acids (**1a, 2a, 5a**) were heated in presence of acetic

anhydride and sodium acetate. This reaction probably starts by a deprotonation of the carboxylic group, followed by the nucleophilic attack of the oxygen to the carbonyl group on the acetic anhydride followed by a subsequent intramolecular cyclization to yield the final cyclic imides. The reaction was quenched with water causing the prompt precipitation of the desired compound. The proposed mechanism of reaction to yield the cyclic imides is exemplified in **Figure 3B**.

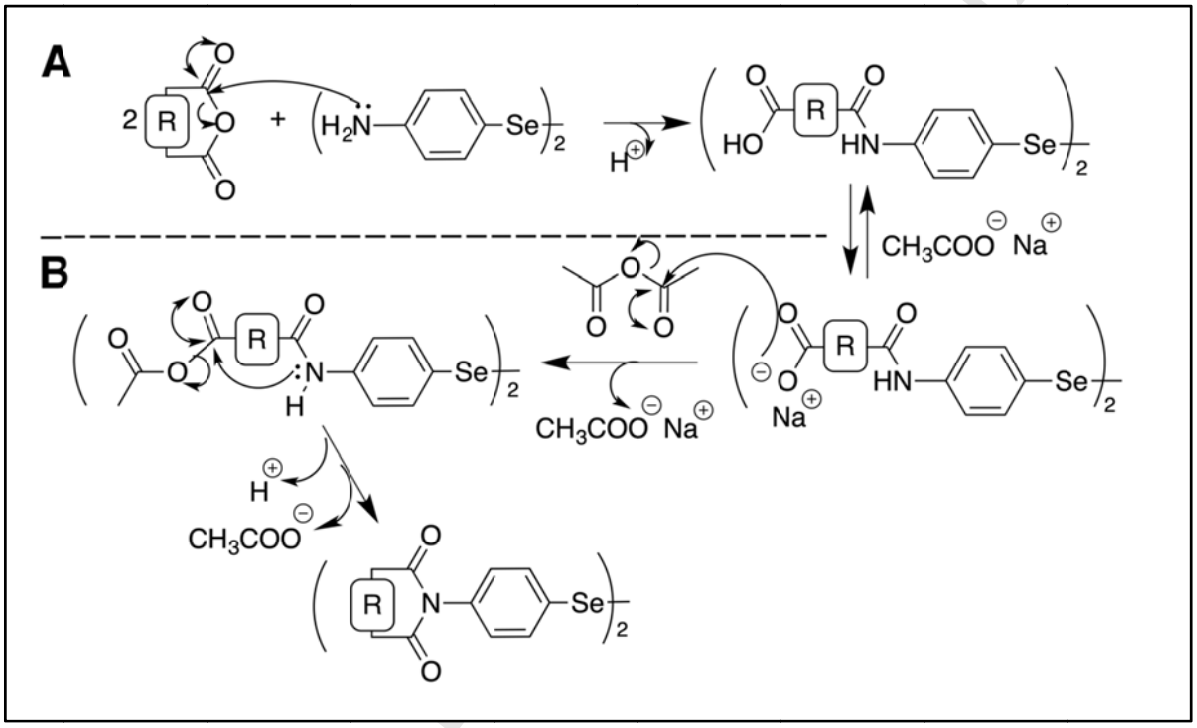

Figure 3. Mechanism proposed for the synthesis diselenide derivatives. Mechanism proposed for the synthesis of compounds **1a-3a**, **5a** and **7a-8a** (**A**). Mechanism proposed for the synthesis of cyclic imide derivatives **9a-11a** (**B**).

2.2. Biology

2.2.1. Cytotoxicity and antiproliferative activity

The cytotoxic potential of the seventeen synthesized compounds was evaluated against a panel of cell lines including seven different cancer cell lines and two other cell lines

derived from non-malignant tissue. Evaluation was performed at 48 h treatment following the MTT (3-(4,5-dimethylthiazol-2-yl)-2,5-diphenyltetrazolium bromide) methodology as previously described [33]. The cancer cell lines included in the panel were PC-3 (prostatic adenocarcinoma); HTB-54 (lung carcinoma), and HT-29 (colon carcinoma); MOLT-4 and CCRF-CEM (acute lymphoblastic leukemia); K-562 (chronic myelogenous leukemia) and MCF-7 (breast adenocarcinoma). The selected cell lines derived from non-malignant tissue were 184B5 and BEAS-2B. Cisplatin was used as positive control. In addition, the parent compounds bis(4-aminophenyl)diselenide (**0a**) and 4-aminophenylselenocyanate (**0b**) were tested as a reference to identify whether the second generation compounds accomplished the objective of improving potency and selectivity.

To narrow down the number of derivatives moving on to the full dose-response cytotoxic profiling assay, a two-dose concentration (100 μM and 10 μM) screening was first performed. The results obtained for the 10 μM treatment are shown in **Figure 4**. As shown in the figure, MCF-7 cells were the most sensitive cells toward the tested derivatives. In fact, seven compounds (**1b**, **2b**, **4b**, **8a**, **8b**, **9a** and **10a**) reduced cell growth to less than 50% when assayed at 10 μM in these cells. Some compounds also matched this threshold in PC-3, CCRF-CEM, HTB-54, MOLT-4 and HT-29 cells. However, none of the derivatives was able to reduce the cell growth effectively in K-562, the most resistant cell line to the treatments. Interestingly, compounds **1b**, **2b**, **4b**, **8a**, **8b**, **9a** and **10a** did not significantly affect cell growth in 184B5 cells, thus suggesting a potential selectivity of the compounds for breast cancer cells. Consequently, those seven compounds were further analysed in full dose-response curves in every cell line. GI_{50}, TGI and LC_{50} values were calculated form the curves and

are shown in **Table 1**. Selectivity for tumor cells was estimated according to the formulas GI_{50} (184B5)/GI_{50} (MCF-7) and GI_{50} (BEAS-2B)/GI_{50}(HTB-54) (**Table 2**).

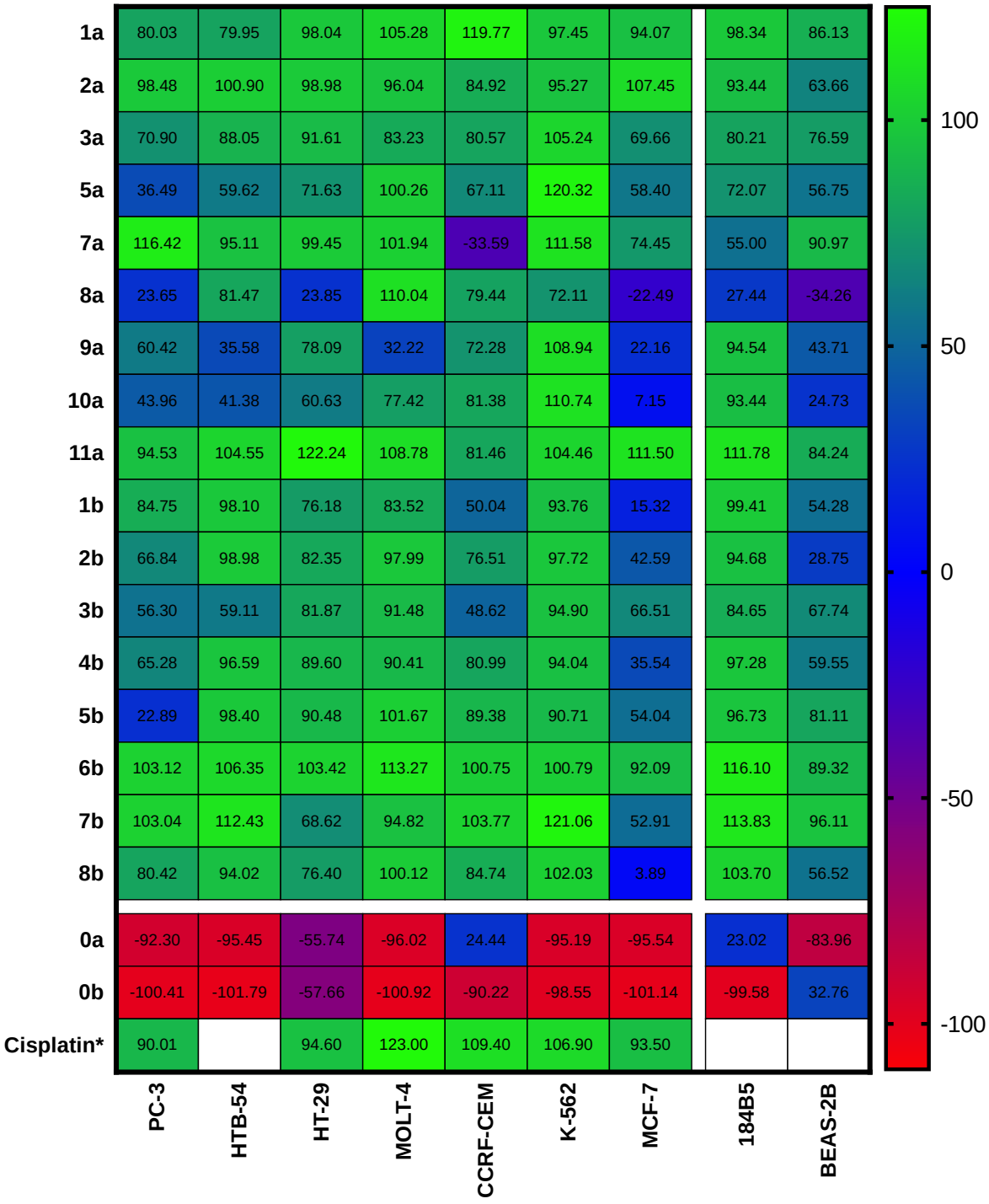

* NCI data (http://dtp.nci.nih.gov).

Figure 4. Heat map representing average percentages of cell growth for every tested structure at a 10 μM concentration for 48 h.

Table 1. Average values of GI_{50}, TGI and LD_{50} (μM) for 48 h treatment.

Code	PC-3			HTB-54			HT-29			MOLT-4			CCRF-CEM			K-562			MCF-7		
	GI_{50}[a]	TGI[b]	LD_{50}[c]	GI_{50}	TGI	LD_{50}	GI_{50}	TGI	LD_{50}	GI_{50}	TGI	LD_{50}	GI_{50}	TGI	LD_{50}	GI_{50}	TGI	LD_{50}	GI_{50}	TGI	LD_{50}
1b	30.44	61.35	92.89	46.95	72.42	93.75	>100	>100	>100	>100	>100	>100	6.77	38.33	91.19	58.58	98.17	>100	1.93	14.83	73.09
2b	19.38	>100	>100	>100	>100	>100	>100	>100	>100	>100	>100	>100	30.16	64.24	95.49	42.82	61.91	88.70	7.71	59.13	>100
4b	68.52	>100	>100	100	>100	>100	>100	>100	>100	>100	>100	>100	46.52	>100	>100	>100	>100	>100	6.47	>100	>100
8a	4.51	17.03	50.55	27.51	55.94	85.49	5.74	33.38	>100	73.77	84.71	94.62	59.13	75.84	>100	25.32	59.67	94.62	7.50	9.18	11.56
8b	21.05	43.22	70.44	47.83	72.42	>100	11.89	42.82	93.75	59.67	69.80	80.15	68.52	>100	>100	67.89	80.15	92.04	3.33	11.56	>100
9a	13.52	36.61	67.89	8.30	14.29	24.18	14.16	20.67	31.01	7.50	15.67	33.69	20.29	47.39	78.69	48.72	69.80	87.08	6.01	11.89	16.57
10a	8.30	33.08	>100	4.91	51.97	>100	11.67	>100	>100	91.19	>100	>100	>100	>100	>100	80.89	>100	>100	0.00096	7.64	>100
0b	1.02	1.54	2.30	0.87	1.00	1.13	0.27	1.11	5.28	3.33	3.39	3.42	1.71	2.74	4.43	1.03	1.29	1.58	1.00	1.48	2.20
0a	0.80	1.62	2.98	0.21	0.80	2.16	<0.01	1.78	8.37	3.84	5.95	8.06	5.28	16.87	42.82	0.95	1.19	1.48	0.75	0.96	1.16
Cisplatin *	5.01	50.1	>100	n.d.[#]	n.d.[#]	n.d.[#]	7.94	>100	>100	1.58	63.10	>100	1.00	79.43	>100	5.01	>100	>100	3.16	>100	>100

[a] GI_{50}, concentration that reduces growth by 50% compared to control. [b] TGI, concentration that completely inhibits cell growth. [c] LC_{50}, concentration that kills 50% of cells. [#] Not determined. * NCI data (http://dtp.nci.nih.gov).

Table 2. Average values of GI_{50}, TGI and LD_{50} (μM) for 48 h treatment and calculated SI.

Code	184B5			SI[a]	BEAS-2B			SI[b]
	GI_{50}	TGI	GI_{50}		GI_{50}	TGI	LD_{50}	
1b	>100	>100	>100	>51.73	10.45	42.82	80.15	0.22
2b	>100	>100	>100	>12.98	4.43	24.63	>100	<0.39
4b	>100	>100	>100	15.46	52.93	>100	>100	<0.16
8a	8.93	11.25	15.67	1.19	1.05	4.43	15.53	0.04
8b	77.25	91.19	>100	23.19	15.82	51.02	77.25	0.33
9a	40.51	63.07	86.29	6.74	1.97	43.62	73.77	0.24
10a	60.78	>100	> 100	6.3×10^4	0.75	20.86	61.91	0.15
0a	6.29	14.03	30.44	8.39	0.73	0.88	1.09	3.44
0b	0.88	1.06	1.27	0.88	7.92	14.69	27.51	9.06

[a] Selectivity index (SI) calculated as GI_{50} (184B5)/GI_{50} (MCF-7). [b] SI calculated as GI_{50} (BEAS-2B)/GI_{50}(HTB-54).

As shown in **Tables 1** and **2**, derivatives **8a**, **9a** and **10a** exhibited GI_{50} values under 10 μM in three of the tested cancer cell lines. Besides, compounds **1b**, **2b**, **4b, 8b** and **10a** were highly selective for tumor cells in the breast model. Remarkably, though highly cytotoxic, parent compounds **0a** and **0b** showed low selectivity for breast cancer cells (SI < 9). Therefore, we decided to focus on the effects of these compounds in the breast cancer cell line. When ranked in terms of potency and selectivity for breast cancer cells, a clear gap established **10a**, a compound with a nanomolar GI_{50} value and a staggering

SI, as the leader structure. Despite less cytotoxic, **1b** and **8b** were also highly selective. Among them, the analog derivative of norcantharidin (**8b**) was selected in order to evaluate whether this structure was able to mimic norcantharidin's effect and induce autophagy. As a result, derivatives **8b** and **10a** were selected to further analyse their mechanism of action in MCF-7 cells. As only the highest concentration tested led to negative growth values as exemplified on **Figure 5**, these results uncover a mainly cytostatic profile.

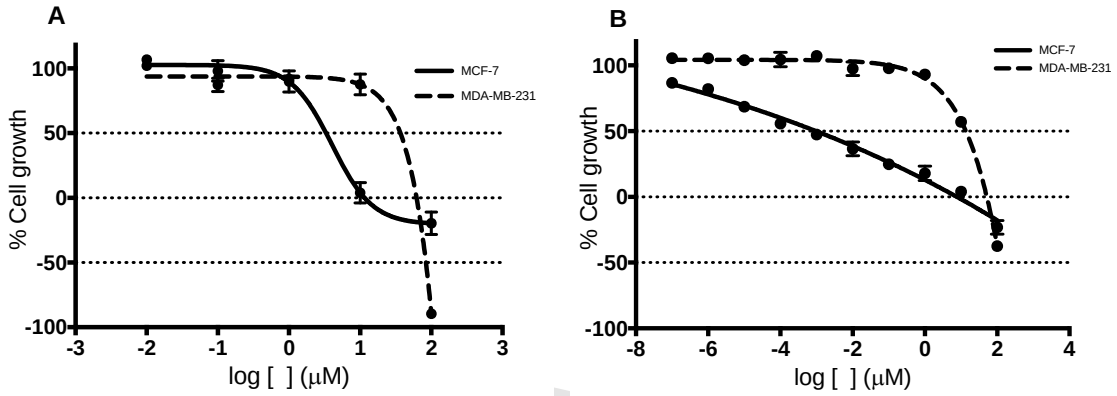

Figure 5. Dose response curves obtained for 8b (A) and 10a (B) in MCF-7 and MDA-MB-231 cell lines.

Besides, comparison between **10a** and **0a** clearly showed a great enhancement in selectivity for the second generation compound. In fact, SI was 7,000 times higher for compound **10a** than for **0a**, its parent compound. This effect was less notorious when compound **8b** was compared with **0b**. However, both **10a** and **8b** succeeded in increasing the selectivity towards the cancer cells, thus meeting one of our goals.

The importance of estrogen receptors (ER) in cell cycle and cell proliferation in breast cancer cells, as well as the crucial role of estradiol synthesis pathways has been widely described. In fact, antiestrogens have been found to repress transcription of several ERα target genes in MCF-7 cells, specifically in S phase [35]. Besides, when MCF-7 cell

cultures were exposed to a genotoxic agent higher levels of DNA damage in *S*- and *G2/M*-enriched cultures correlated with higher levels of CYP1A1 y CYP1B1 [36]. MCF-7 is an ERα expressing cell line. Therefore, to compare we decided to test **8b** and **10a** in MDA-MB-231, a breast cancer cell line non-expressing ERα. Obtained results for MDA-MB-231 cells are shown in **Figure 5**. As shown in the figure, **8a** and **10a** dose-response curves in MDA-MB-231differ from those obtained in MCF-7 cells. Moreover, lying in the micromolar range GI_{50}, TGI and LD_{50} values for **8b** (GI_{50}= 33.61 μM, TGI= 61.92 μM and LD_{50}= 83.92 μM) and **10a** (GI_{50}= 13.65 μM, TGI= 51.49 μM and LD_{50}> 100 μM) are also higher than in MCF-7cells. These data suggest that ER signalling and/or estradiol metabolism play a relevant role in cytostatic effect displayed by **8b** and **10a** in MCF-7 cells.

In terms of structure-activity relationship, most diselenide structures containing carboxylic moieties were discarded in the screening process. For instance, when comparing **8b** with its diselenide homolog a complete loss of selectivity could be observed. On the other hand, if we stablish a comparison between carboxylic derivatives and their cyclic imide homologs data suggests that this modification was crucial for both potency and selectivity.

*2.2.2. Compounds **8b** and **10a** induce cell cycle arrest in S phase and cell death*

Many selenium containing compounds involve cell cycle regulation among their therapeutic effects [13]. Therefore, as a first approach to the mechanism of action we studied the effect of **8b** and **10a** on cell cycle. With this purpose, the cell cycle status of MCF-7 cell cultures treated with different concentrations of **8b** and **10a** and for different time points was determined by flow cytometry. Camptothecin was used as positive control. As shown in the **Figure 6**, both a reduction in the number of G_0/G_1 cells and a significant increase in the percentage of cells in S phase were detected for

both compounds even at the lowest concentration (10 μM) and the shortest time tested (24 h). This result, indicative of S phase arrest was both dose (**Figure 6A**) and time (**Figures 6B** and **C**) dependent.

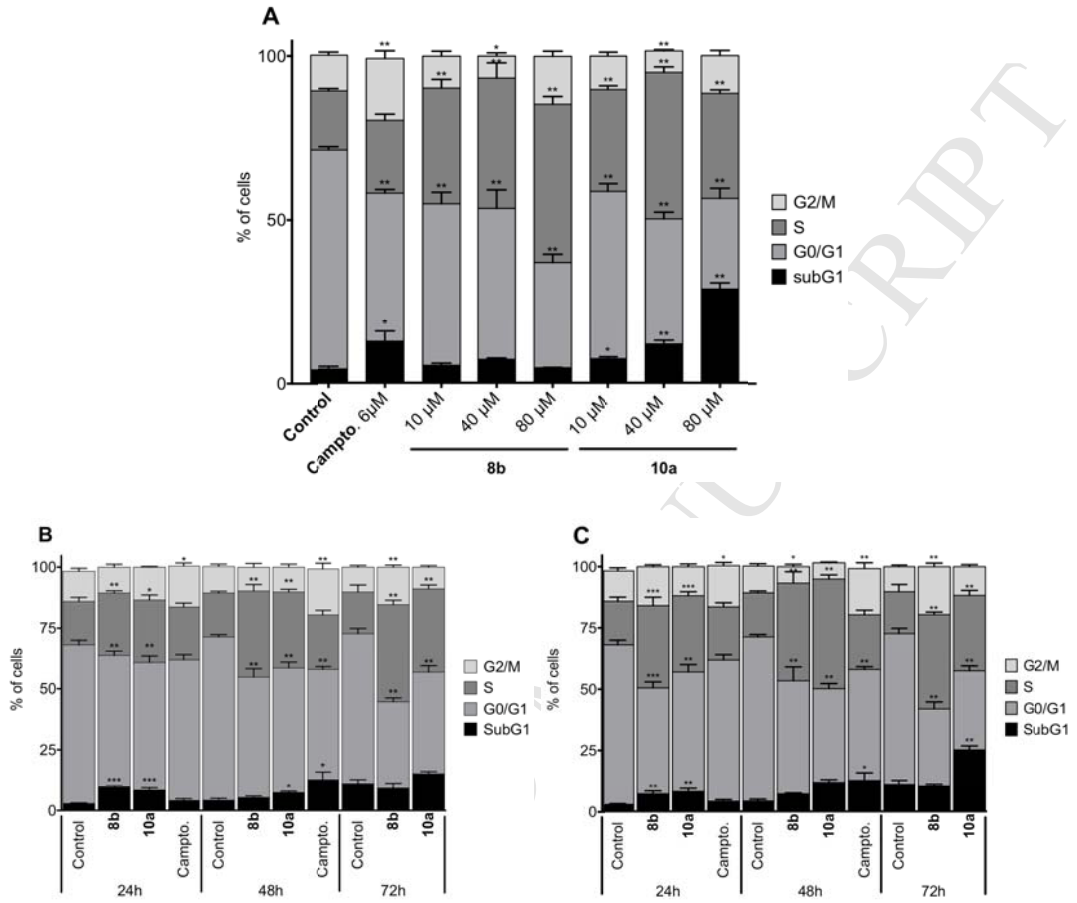

Figure 6. Cell cycle phase distribution of MCF-7 cell cultures after treatment with compounds 8b and 10a. (**A**) Dose-dependent induction of cell cycle arrest after 48 h treatment with compounds **8b** and **10a**. Time-course analysis of cell cycle distribution at 10 μM (**B**) and 40 μM (**C**) of **8b** and **10a**. Camptothecin (6 μM) was employed as a positive control. Results are expressed as a mean ± SEM of at least three independent experiments performed in duplicate. *$p < 0.05$, **$p < 0.01$ and ***$p < 0.001$ compared to control cells.

To study the role of apoptosis in the induction of cell death by **8b** and **10a**, MCF-7 cells were incubated in the presence of increasing concentrations of **8b** and **10a** for 48 h. Then, the apoptotic status of the cells was studied by TUNEL. As shown in **Figure 7A**, when tested at concentrations higher than 40 μM, both compounds induced a significant increase in the number of death cells (subdiploid cells). **Figure 7B** shows that at 40 μM concentration the induction of cell death could be detected as soon as 24 h.

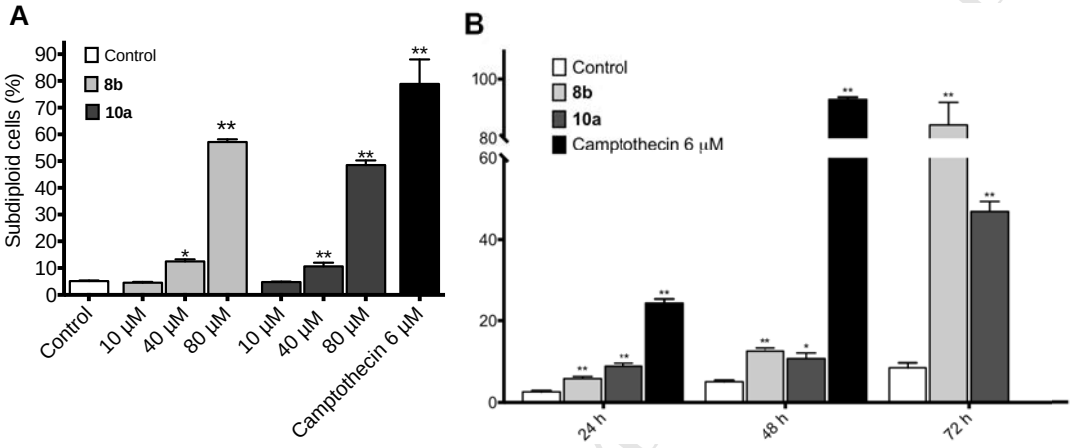

Figure 7. Compounds 8b and 10a induced cell death in a dose- and time-dependent manner in MCF-7 cell cultures. Cells were treated with increasing concentrations of compounds **8b** and **10a** for 48 h (**A**) or at 40 μM concentration for different periods of time (**B**). Camptothecin was used as positive control. Results are expressed as a mean ± SEM of at least three independent experiments performed in duplicate. *$p < 0.05$ and **$p < 0.01$ compared to control cells.

*2.2.3. Compounds **8b** and **10a** induce autophagy-mediated cell death and AMPK/JNK pathway activation*

To further analyse the molecular mechanism by which **8b** and **10a** reduced MCF-7 cell viability, we explored the effect of pre-treatment of the cultures with either an autophagy inhibitor (wortmannin, chloroquine) [37-39] or a pan-caspase inhibitor (Z-

VAD-FMK) on the induction of cell death by these compounds. As shown in **Figure 8**, pre-treatment of the cells with the PI3K inhibitor wortmannin or the lysosomal inhibitor chloroquine led to a significant reduction in the number of dead cells in the cultures after exposure to compounds **8b** and **10a**. However, pre-incubation of **t**he cultures with Z-VAD-FMK could not prevent **8b** and **10a**-induced cell death. These results suggest that autophagy is the way by which **8b** and **10a** cause their effect.

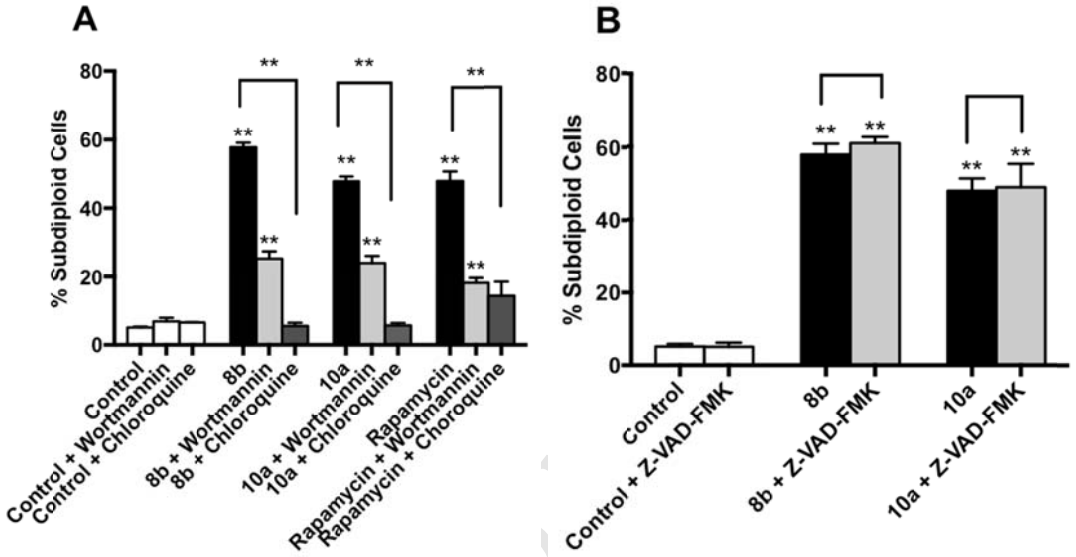

Figure 8. Cell death induced by compounds 8b and 10a is partially blocked by wortmannin or chloroquine but not by caspase inhibitor Z-VAD-FMK. Cell death determination in MCF-7 cell cultures pre-incubated with (**A**) 100 nM wortmannin, 10 μM chloroquine or (**B**) 50 mM Z-VAD-FMK before treatment with 80 μM **8b**, 80 μM **10a** or 30 μM rapamycin for 48 h. Rapamycin was used as reference autophagy control at 30 μM treatment. Results are expressed as a mean ± SEM of at least three independent experiments performed in duplicate. *$p < 0.05$ and **$p < 0.01$ compared to the control.

To further confirm the involvement of autophagy in **8b** and **10a** induced cell death the levels of expression of the autophagy markers Beclin-1 and LC3B were determined. Autophagic flux was also assessed by testing SQSTM1/p62 [40]. As shown in **Figure 9**, when MCF-7 cells were treated with 80 μM of either compound for 48 h, Beclin-1, LC3B-I and LC3B-II were augmented while SQSTM1/p62 was downregulated thus confirming autophagy. Since the activation of AMPK and JNK have been shown to play a role in autophagy-mediated cell death [6, 41], AMPK and JNK phosphorylation were also studied. As shown in **Figure 9**, both **8b** and **10a** induced AMPK and JNK phosphorylation.

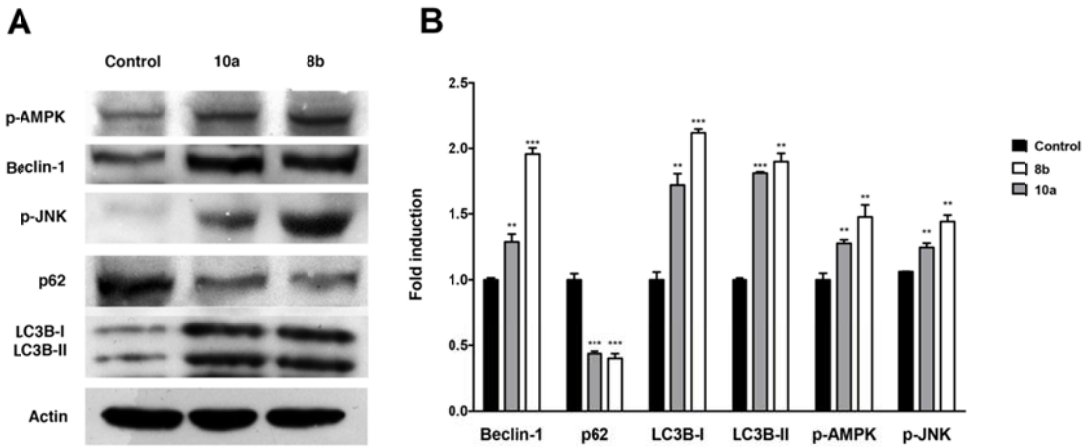

Figure 9. Beclin-1, p62, LC3B-I, LC3B-II, p-AMPK and p-JNK proteins were determined by western blot. (**A**) A representative experiment is exemplified. (**B**) Aggregate results (mean ± SEM; n=3) expressed as fold induction relative to control cells. *$p < 0.05$, **$p < 0.01$ and ***$p < 0.001$.

Inhibition of mTORC1 after AMPK activation is a main step in AMPK-mediated autophagy. The PI3K/AKT pathway also has a regulatory effect on mTOR and therefore in autophagy. This pathway is commonly deregulated in cancer cells [42]. Aimed to

analyze the effect of **8b** and **10a** on PI3K and AKT signaling, we determined the phosphorylation status of both, the PI3K catalytic subunit p110α and AKT (Ser473). As shown in **Figure 10**, increased phospho-p110α and phospho-AKT (Ser473) were detected indicating activation of the pathway. PI3K activation is usually related to tumor migration enhancement [43] and has been reported to be associated with inhibition of autophagy and tumorgenesis [44]. However, in the specific context of breast adenocarcinoma cells PI3K activation does not necessarily lead to autophagy suppression [45]. Moreover, specific activation of the isoform 1 of AKT in breast, neck and head carcinomas has been shown to interfere with their metastatic progression [46, 47]. Whether AKT-mediated repression of metastasis would represent an additional beneficial effect of the treatment with compounds **8b** and **10a** merits further research.

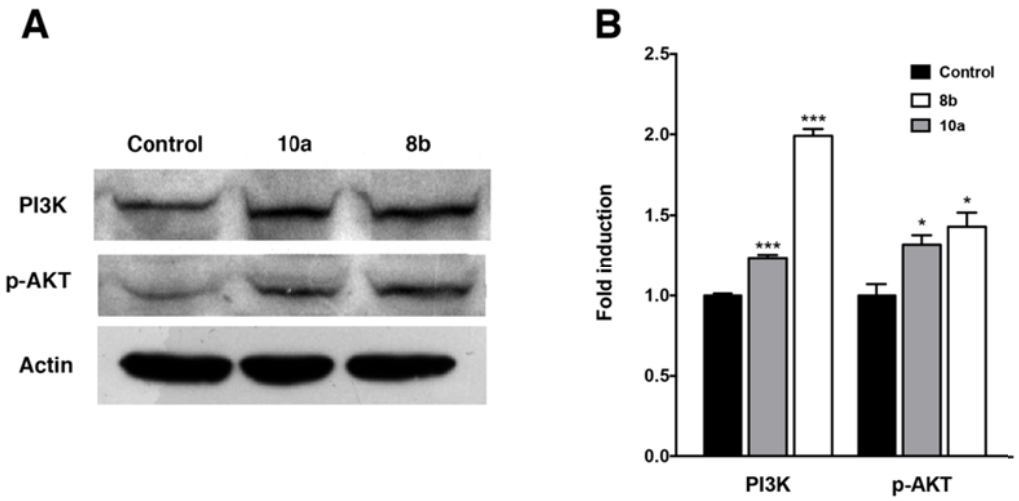

Figure 10. PI3K and p-AKT proteins were determined by western blot. (**A**) A representative experiment is exemplified. (**B**) Aggregate results (mean ± SEM; n=3) expressed as fold induction relative to control cells. *p < 0.05, **p < 0.01 and ***p < 0.001.

3. Conclusion

To sum up, nine diselenide (**1a-3a**, **5a**, **7a-11a**) and eight selenocyanate monoamidic acids (**1b-8b**) were synthesized with high yields. A screening in a panel of cancer cell lines revealed that MCF-7 was the most sensitive among the tested ones to treatment with these compounds. Due to their high potency and stunning selectivity towards MCF-7 cells, derivatives **8b** and **10a** emerged as the most promising structures. Full dose response curves in MCF-7 cells showed up a cytostatic effect for these compounds. Further analysis uncovered their ability to induce both S phase arrest and a caspase-independent cell death program in these cells. Besides, wortmannin and chloroquine partially prevented induction of cell death, thus suggesting autophagy. Increased levels of Beclin1 and LC3-IIB and reduced levels of SQSTM1/p62 in MCF-7 cells after exposure to **8b** or **10a** also supported autophagy. Since pJNK upregulation and AMPK phosphorylation were also detected after the treatments, the modulation of the AMPK and JNK signaling pathways seems to be involved in the induction of autophagy by **8b** and **10a**. Finally, the phosphorylation of both, AKT and the PI3K catalytic subunit p110α were also detected. Whether the activation of the PI3K/AKT pathway by **8b** and **10a** in MCF-7 cells restricts their invasive capacity and represents an extra beneficial effect of these compounds for cancer treatment deserves to be studied profoundly.

4. Experimental

4.1. Chemistry

4.1.1. Material and methods

Proton (^{1}H) and carbon (^{13}C) NMR spectra of every compound and selenium (^{77}Se) NMR spectra of representative derivatives were recorded on a Bruker Advance Neo 400

Ultrashield™ spectrometer (Rheinstetten, Germany) using DMSO-d_6 as solvent. IR spectra were recorded on a Thermo Nicolet FT- IR Nexus spectrophotometer using KBr pellets for solid samples. Elemental analysis was performed on a LECO CHN-900 Elemental Analyzer. Purity of all final compounds was 95% or higher. Chemicals were purchased from E. Merck (Darmstadt, Germany), Panreac Química S.A. (Montcada i Reixac, Barcelona, Spain), Sigma-Aldrich Quimica, S.A. (Alcobendas, Madrid, Spain) and Acros Organics (Janssen Pharmaceuticalaan, Geel, Belgium).

*4.1.2. General procedure for the synthesis of compounds **1a-3a**, **5a** and **7a-8a***

Bis(4-aminophenyl)diselenide (1 mmol) was dissolved in of dry acetone (10 mL) and the corresponding anhydride (2.1 mmol) then added. The reaction was then stirred for a variable time of 8 h up to 24 h at room temperature. Then reaction was quenched with water, compound was filtered and purified by stirring or washing with ethyl ether.

In order to assign the chemical shifts in NMR spectroscopy the following assignment has been done: central rings A and A', external fragments B and B' (**Figure 11**).

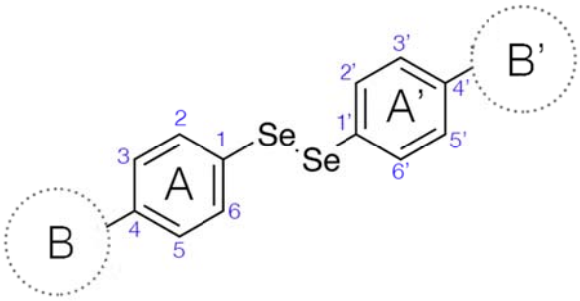

Figure 11. General NMR assignation for compounds of series a.

*4.1.2.1. (2Z,2'Z)-4,4'-[diselenodiylbis(benzene-4,1-diylimino)]bis(4-oxobut-2-enoic acid) (**1a**)*

From maleic anhydride. Conditions: 8 h at room temperature. The product was kept under stirring with water (25 mL) for 2 h, filtered and then washed with ethyl ether (2 × 25 mL). A yellow powder was obtained. Yield: 68.9%. Mp: 186–186.5ºC. IR (KBr) cm^{-1}: 3305, 3193 (N-H), 1723 (C=O carboxylic acid), 1623 (C=O, amide), 818 (Se-Se). ^{1}H NMR (400 MHz, DMSO-d_6) δ: 13.01 (bs, 2H, COOH), 10.54 (s, 2H, NH), 7.60 (d, 4H, A+A', J_{2-3}=J_{6-5}= 8.8 Hz, H_2+H_6), 7.57 (d, 4H, A+A', J_{3-2}=J_{5-6}= 8.8 Hz, H_3+H_5), 6.46 (d, 2H, B+B', J_{1-2}= 12.0 Hz, H_1), 6.31 (d, 2H, B+B', J_{2-1}= 12.0 Hz, H_2). ^{13}C NMR (100 MHz, DMSO-d_6) δ: 166.76 (COOH), 163.17 (C=O), 138.71 (A+A', C_4), 132.88 (A+A', C_2+C_6), 131.33+130.23 (B+B', C_1+C_2), 124.19 (A+A', C_1), 120.02 (A+A', C_3+C_5). MS [*m/z* (% abundance)]: 172 (100), 344 (25). Elemental analysis calculated (%) for $C_{20}H_{16}N_2O_6Se_2 \cdot 2H_2O$: C: 41.83, H: 3.51, N: 4.88; found: C: 41.54, H: 3.53, N: 4.80.

4.1.2.2. 2,2'-[(Diselenodiyldibenzene-4,1-diyl)dicarbamoyl]bis(benzoic acid) ***(2a)***

From phthalic anhydride. Conditions: 12 h at room temperature. The product was kept under stirring with water (25 mL) for 1 h, filtered and then washed with ethyl ether (2 × 25 mL). A yellow powder was obtained. Yield: 26.7%. Mp: 154–155ºC. IR (KBr) cm^{-1}: 3282 (N-H),1708 (C=O carboxylic acid), 1657 (C=O, amide), 819 (Se-Se). ^{1}H NMR (400 MHz, DMSO-d_6) δ: 11.02 (s, 2H, NH), 7.85 (d, 2H, B+B', J_{3-4}= 8.8 Hz, H_3), 7.72–7.66 (m, 4H, B+B', H_4+H_6), 7.63–7.52 (m, 10H, A+A', H_2+H_3+H_4+H_5, B+B', H_5), 3.39 (bs, H_2O+2COOH). ^{13}C NMR (100 MHz, DMSO-d_6) δ: 171.22 (COOH), 168.50 (C=O), 140.48 (A+A', C_4), 134.06+132.02 (A+A', C_2+C_6+C_1), 130.40+130.27 (B+B', C_5+C_4), 128.65+126.48 (B+B', C_1+C_2), 124.60 (A+A', C_3+C_5), 121.03+120.51 (B+B', C_3+C_6). ^{77}Se NMR (76 MHz, DMSO-d_6) δ: 482.83 (Se-Se). MS [*m/z* (% abundance)]: 104 (100), 172 (93), 344 (25). Elemental analysis calculated (%) for $C_{28}H_{20}N_2O_6Se_2 \cdot 2H_2O$: C: 49.87, H: 3.59, N: 4.15; found: C: 49.73, H: 3.53, N: 4.35.

*4.1.2.3. 4,4'-[Diselenodiylbis(benzene-4,1-diylimino)]bis(4-oxobutanoic acid) (**3a**)*

From succinic anhydride. Conditions: 24 h at room temperature. The product was kept under stirring with water (25 mL) for 2 h, filtered, then stirred with ethyl ether (100 mL) for 24 h and then filtered. A yellow powder was obtained. Yield: 72.27%. Mp: 179–180ºC. IR (KBr) cm^{-1}: 3318 (NH), 1696 (C=O carboxylic acid), 1666 (C=O, amide), 818 (Se-Se). ^{1}H NMR (400 MHz, DMSO-d_6) δ: 12.21 (bs, 2H, COOH), 10.11 (s, 2H, NH), 7.56 (d, 4H, A+A', $J_{2\text{-}3}$= $J_{6\text{-}5}$= 8.4 Hz, H_2+H_6), 7.51 (d, 4H, A+A', $J_{3\text{-}2}$= $J_{5\text{-}6}$= 8.4 Hz, H_3+H_5), 2.60–2.46 (m, 8H, B+B', H_1+H_2). ^{13}C NMR (100 MHz, DMSO-d_6) δ: 174.27 (COOH), 170.80 (C=O), 140.09 (A+A', C_4), 133.76 (A+A', C_2+C_6), 123.85 (A+A', C_1), 120.12 (A+A', C_3+C_5), 31.57+29.23 (B+B', C_2+C_1). MS [*m/z* (% abundance)]: 172 (100), 344 (15), 424 (10). Elemental analysis calculated (%) for $C_{20}H_{20}N_2O_6Se_2 \cdot 2H_2O$: C: 41.51, H: 4.18, N: 4.84; found: C: 41.11, H: 3.79, N: 4.77.

*4.1.2.4. 2,2'-[(Diselenodiylbis(benzene-4,1-diylimino)]bis(2-oxoethane-2,1-diyloxy)diacetic acid (**5a**)*

From diglycolic anhydride. Conditions: 24 h at room temperature. The product was kept under stirring with water (25 mL) for 2 h, filtered, then stirred with ethyl ether (100 mL) for 24 h and then filtered. A yellow powder was obtained. Yield: 69.7%. Mp: 140–141ºC. IR (KBr) cm^{-1}: 3337 (NH), 1709 (C=O carboxylic acid), 1683 (C=O, amide), 818 (Se-Se). ^{1}H NMR (400 MHz, DMSO-d_6) δ: 12.76 (bs, 2H, COOH), 10.09 (s, 2H, NH), 7.62 (d, 4H, A+A', $J_{2\text{-}3}$= $J_{6\text{-}5}$= 8.5 Hz, H_2+H_6), 7.55 (d, 4H, A+A', $J_{3\text{-}2}$= $J_{5\text{-}6}$= 8.5 Hz, H_3+H_5), 4.19 (s, 4H, B+B', H_1), 4.17 (s, 4H, B+B', H_2). ^{13}C NMR (100 MHz, DMSO-d_6) δ: 172.68 (COOH), 168.99 (C=O), 139.56 (A+A', C_4), 133.94 (A+A', C_2+C_6), 125.01 (A+A', C_1), 121.22 (A+A', C_3+C_5), 71.38+69.11 (B+B', C_2+C_1). MS

[*m/z* (% abundance)]: 93 (95), 172 (100). Elemental analysis calculated (%) for $C_{20}H_{20}N_2O_8Se_2$: C: 41.83, H: 3.51, N: 4.88; found: C: 41.83, H: 3.82, N: 5.19.

*4.1.2.5. 2,2'-[(Diselenodiyldibenzene-4,1-diyl)dicarbamoyl]bis(cyclohexanecarboxylic acid) (**7a**)*

From *cis*-1,2-cyclohexanecarboxylic anhydride. Conditions: 24 h at room temperature. The product was kept under stirring with water (25 mL) for 2 h, filtered, then stirred with ethyl ether (100 mL) for 24 h and then filtered. A light brown powder was obtained. Yield: 97.7%. Mp: 150–151ºC. IR (KBr) cm^{-1}: 3307 (NH), 1698 (C=O carboxylic acid), 1665 (C=O, amide), 820 (Se-Se). ^{1}H NMR (400 MHz, DMSO-d_6) δ: 11.88 (bs, 2H, COOH), 9.87 (s, 2H, NH), 7.55 (d, 4H, A+A', $J_{2\text{-}3}$=$J_{6\text{-}5}$= 8.8 Hz, H_2+H_6), 7.50 (d, 4H, A+A', $J_{3\text{-}2}$=$J_{5\text{-}6}$= 8.8 Hz, H_3+H_5), 2.93 (d, 2H, B+B', $J_{1\text{-}CHchex}$= 5.4 Hz, H_1), 2.70–2.56 (m, 2H, B+B', H_{chex}), 2.09 (d, 2H, B+B', $J_{CHchex\text{-}1}$ = 5.4 Hz, H_{chex}), 1.98 (d, 2H, B+B', *J*= 8.9 Hz, H_{chex}), 1.83–1.57 (m, 6H, B+B', 3H_{chex}), 1.48–1.24 (m, 6H, B+B', 3H_{chex}). ^{13}C NMR (100 MHz, DMSO-d_6) δ: 175.56 (COOH), 173.36 (C=O), 140.42 (A+A', C_4), 133.78 (A+A', C_2+C_6), 123.66 (A+A', C_1), 120.26 (A+A', C_3+C_5), 43.00+42.44 (B+B', C_1+C_2), 28.13+25.62+24.47+22.78 (B+B', C_3+C_4+C_5+C_6). MS [*m/z* (% abundance)]: 81 (70), 172 (100), 344 (25). Elemental analysis calculated (%) for $C_{28}H_{32}N_2O_6Se_2$: C: 51.70, H: 4.96, N: 4.31; found: C: 52.06, H: 5.09, N: 4.71.

*4.1.2.6. 3,3'-[(Diselenodiyldibenzene-4,1-diyl)dicarbamoyl]bis(7-oxabicyclo[2.2.1]hept-5-ene-2-carboxylic acid) (**8a**)*

From 3,6-epoxy-1,2,3,6-tetrahydrophthalic anhydride obtained by the classic procedure described for a Diels-Alder reaction using furan and maleic anhydride as reagents to yield the Diels-Alder adduct. Conditions: 24 h at room temperature. The product was

kept under stirring with water (25 mL) for 2 h, filtered, then stirred with ethyl ether (100 mL) for 24 h and then filtered. A yellow powder was obtained. Yield: 22.5%. Mp: 126–127ºC IR (KBr) cm^{-1}: 3299 (NH), 1706 (C=O carboxylic acid), 1669 (C=O, amide), 819 (Se-Se). ^{1}H NMR (400 MHz, DMSO-d_6) δ: 12.19 (bs, 2H, COOH), 10.03 (s, 2H, NH), 7.65 (d, 4H, A+A', J_{2-3}=J_{6-5}= 9.0 Hz, H_2+H_6), 7.62 (d, 4H, A+A', J_{3-2}=J_{5-6}= 9.0 Hz, H_3+H_5), 6.50 (s, 4H, B+B', H_3+H_5), 5.14 (s, 2H, B+B', H_5), 5.06 (s, 2H, B+B', H_2), 2.82 (d, 2H, B+B', J_{1-6}= 9.1 Hz, H_1), 2.71 (d, 2H, B+B', J_{6-1}= 9.1 Hz, H_6). ^{13}C NMR (100 MHz, DMSO-d_6) δ: 173.08 (COOH), 170.48 (C=O), 141.07 (A+A', C_4), 137.49+137.08 (B+B', C_4+C_5), 135.29 (A+A', C_2+C_6), 120.79 (A+A', C_1), 116.51 (A+A', C_3+C_5), 80.82+79.61 (B+B', C_3+C_6), 47.96+47.36 (B+B', C_1+C_2). MS [*m/z* (% abundance)]: 172 (100), 344 (25). Elemental analysis calculated (%) for $C_{28}H_{24}N_2O_8Se_2 \cdot 2H_2O$: C: 47.34, H: 3.97, N: 3.94; found: C: 47.66, H: 4.13, N: 4.23.

*4.1.3. General procedure for the synthesis of compounds **9a–11a***

A reaction mixture containing 1.3 mmol of the corresponding carboxylic derivatives (**1a**, **2a** or **5a**) in 15 mL of acetic anhydride and 200 mg of sodium acetate was heated for 3 h under reflux, then quenched with water (50 mL) and kept under stirring for 3 h. The aqueous solution was extracted with CH_2Cl_2 (2 × 25 mL), dried with sodium sulphate anhydrous and the solvent was evaporated under vacuum.

*4.1.3.1. 1,1'-(Diselenediyldibenzene-4,1-diyl)bis(1H-pyrrole-2,5-dione) (**9a**)*

From compound **1a**. The product was then washed with *n*-hexane (100 mL). A yellow solid was obtained. Yield: 55.4%. Mp: 91.5–92.5ºC. IR (KBr) cm^{-1}: 1710 (C=O), 818 (Se-Se). ^{1}H NMR (400 MHz, DMSO-d_6) δ: 7.77 (d, 4H, A+A', J_{2-3}=J_{6-5}= 8.6 Hz, H_2+H_6), 7.33 (d, 4H, A+A', J_{3-2}=J_{5-6}= 8.6 Hz, H_3+H_5), 7.19 (s, 4H, B+B', H_1+H_2). ^{13}C

NMR (100 MHz, DMSO-d_6) δ: 169.69 (C=O), 134.75 (A+A', C_4), 131.37+131.27 (A+A', C_2+C_6; B+B', C_1+C_2), 129.15 (A+A', C_1), 127.51 (A+A', C_3+C_5). MS [m/z (% abundance)]: 57 (75), 252 (100), 311 (65). Elemental analysis calculated (%) for $C_{20}H_{12}N_2O_4Se_2 \cdot H_2O$: C: 46.17, H: 2.71, N: 5.38; found: C: 46.10, H: 3.03, N: 4.94.

*4.1.3.2. 1,1'-(Diselenodiyldibenzene-4,1-diyl)bis(1H-isoindole-1,3(2H)-dione) (**10a**)*

From compound **2a**. The product was then washed with *n*-hexane (100 mL). A yellow solid was obtained. Yield: 90.6%. Mp: 248–249ºC. IR (KBr) cm^{-1}: 1709 (C=O), 815 (Se-Se). ^{1}H NMR (400 MHz, DMSO-d_6) δ: 8.15–7.79 (m, 12H, A+A', H_2+H_6; B+B', H_2+H_3+H_4+H_5), 7.55 (d, 4H, A+A', $J_{3\text{-}2}$=$J_{5\text{-}6}$= 8.4 Hz, H_3+H_5). ^{13}C NMR (100 MHz, DMSO-d_6) δ: 172.73 (C=O), 140.18+140.09 (A+A', C_4; B+B', C_1+C_6), 133.49 (B+B', C_4+C_5), 131.99+131.73 (A+A', C_1+C_2+C_6), 128.65 (B+B', C_2+C_5), 120.26 (A+A', C_3+C_5). ^{77}Se NMR (76 MHz, DMSO-d_6) δ: 481.88 (Se-Se). MS [*m/z* (% abundance)]: 93 (65), 172 (100), 302 (15), 604 (5). Elemental analysis calculated (%) for $C_{28}H_{16}N_2O_4Se_2 \cdot 2H_2O$: C: 52.68, H: 3.16, N: 4.39; found: C: 52.82, H: 3.20, N: 4.77.

*4.1.3.3. 1,1'-(Diselenodiyldibenzene-4,1-diyl)bis(morpholine-3,5-dione) (**11a**)*

From compound **5a**. The product was then washed with ethyl ether (3 × 10 mL). A yellow solid was obtained. Yield: 72.6%. MP: 150–152. IR (KBr) cm^{-1}: 1708 (C=O), 819 (Se-Se). ^{1}H NMR (400 MHz, DMSO-d_6) δ: 7.76 (d, 4H, A+A', $J_{2\text{-}3}$=$J_{6\text{-}5}$= 7.8 Hz, H_2+H_6), 7.23 (d, 4H, A+A', $J_{3\text{-}2}$=$J_{5\text{-}6}$= 7.8 Hz, H_3+H_5), 4.54 (s, 8H, B+B', H_2+H_3). ^{13}C NMR (100 MHz, DMSO-d_6) δ: 170.19 (C=O), 133.32 (A+A', C_4), 131.42 (A+A', C_2+C_6), 130.71 (A+A', C_1), 130.30 (A+A', C_3+C_5), 67.74 (B+B', C_1+C_2). MS [*m/z* (% abundance)]: 184 (100), 271 (25), 538 (15). Elemental analysis calculated (%) for $C_{20}H_{16}N_2O_6Se_2 \cdot H_2O$: C: 43.18, H: 3.26, N: 5.04; found: C: 43.45, H: 3.52, N: 5.36.

4.1.4. General procedure for the synthesis of compounds ***1b–8b***

4-Aminophenyl selenocyanate (2 mmol) was dissolved in dry acetone (15 mL) and the corresponding anhydride (2 mmol) then added. The reaction was then stirred for a variable time of 12 h up to 48 h at room temperature. Reaction was quenched with water, compound was then filtered and purified by stirring or washing with solvents such as *n*-hexane and ethyl ether. The chemical shifts assignment in NMR spectroscopy for these compounds is exemplified in **Figure 12**.

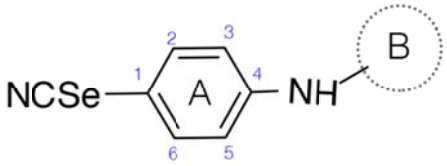

Figure 12. NMR assignation rules followed for series b.

*4.1.4.1. (2Z)-4-oxo-4-[(4-selenocyanatophenyl)amino]but-2-enoic acid (**1b**)*

From maleic anhydride. Conditions: 14 h at room temperature. The product was kept under stirring with water (25 mL) for 2 h, filtered and then washed with *n*-hexane (25 mL) and ethyl ether (25 mL). A yellow powder was obtained. Yield: 51.8%. Mp: 161–162ºC. IR (KBr) cm^{-1}:3299, 3196 (N-H), 2157 (CN), 1722 (C=O carboxylic acid), 1624 (C=O, amide). ^{1}H NMR (400 MHz, DMSO-d_6) δ: 12.96 (s, 1H, COOH), 10.58 (s, 1H, NH), 7.69 (bs, 4H, A, H_2+H_3+H_5+H_6), 6.47 (d, 1H, B, $J_{1\text{-}2}$= 12.0 Hz, H_1), 6.33 (d, 1H, B, $J_{2\text{-}1}$= 12.0 Hz, H_2). ^{13}C NMR (100 MHz, DMSO-d_6) δ: 167.37 (COOH), 164.02 (C=O), 140.42 (A, C_4), 135.24 (A, C_2+C_6), 132.04+130.75 (B, C_1+C_2), 121.16 (A, C_3+C_5), 117.57 (A, C_1), 105.77 (CN). ^{77}Se NMR (76 MHz, DMSO-d_6) δ: 322.45 (SeCN). MS [*m/z* (% abundance)]: 118 (100), 198 (25), 278 (10), 296 (7). Elemental

analysis calculated (%) for $C_{11}H_8N_2O_3Se$: C: 44.74, H: 2.73, N: 9.49; found: C: 44.35, H: 3.08, N: 9.10.

*4.1.4.2. 2-[(4-Selenocyanatophenyl)carbamoyl]benzoic acid (**2b**)*

From phthalic anhydride. Conditions: 14 h at room temperature. The product was kept under stirring with water (25 mL) for 2 h, filtered and then washed with *n*-hexane (25 mL) and ethyl ether (25 mL). A white powder was obtained. Yield: 89.5%. Mp: 162–164ºC. IR (KBr) cm^{-1}: 3317, 3122 (N-H), 2149 (CN), 1718 (C=O carboxylic acid), 1647 (C=O, amide). ^{1}H NMR (400 MHz, DMSO-d_6) δ: 13.14 (s, 1H, COOH), 10.60 (s, 1H, NH), 7.92 (d, 1H, B, $J_{3\text{-}4}$= 7.5 Hz, H_3), 7.78 (d, 2H, A, $J_{2\text{-}3}$=$J_{6\text{-}5}$= 8.3 Hz, H_2+H_6), 7.73–7.64 (m, 3H, A, H_3+H_5, B, H_4), 7.62–7.54 (m, 2H, B, H_5+H_6). ^{13}C NMR (100 MHz, DMSO-d_6) δ: 168.23 (COOH), 167.80 (C=O), 141.32+139.03 (A, C_4; B, C_1), 135.29 (A, C_2+C_6), 132.31 (B, C_5), 130.30+130.09+130.05 (B, C_2+C_3+C_4), 128.25 (B, C_6), 121.16 (A, C_1), 116.99 (A, C_3+C5), 105.91 (CN). MS [*m/z* (% abundance)]: 76 (50), 104 (55), 118 (100), 198 (20). Elemental analysis calculated (%) for $C_{15}H_{10}N_2O_3Se$: C: 52.19, H: 2.92, N: 8.11; found: C: 52.06, H: 3.24, N: 8.06.

*4.1.4.3. 4-Oxo-4-[(4-selenocyanatophenyl)amino]butanoic acid (**3b**)*

From succinic anhydride. Conditions: 24 h at room temperature. The product was kept under stirring with water (25 mL) for 2 h, filtered, then stirred with ethyl ether (100 mL) for 24 h and then filtered. A brown powder was obtained. Yield: 36.7%. Mp: 154–156ºC. IR (KBr) cm^{-1}: 3340 (NH), 2158 (CN), 1693 (C=O carboxylic acid), 1636 (C=O, amide). ^{1}H NMR (400 MHz, DMSO-d_6) δ: 12.18 (bs, 1H, COOH), 10.21 (s, 1H, NH), 7.66 (bs, 4H, A, H_2+H_6+H_3+H_5), 2.58 (d, 2H, A, $J_{2\text{-}1}$= 6.0 Hz, H_2), 2.54 (d, 2H, A, $J_{1\text{-}2}$= 6.0 Hz, H_1). ^{13}C NMR (100 MHz, DMSO-d_6) δ: 174.27 (COOH), 171.03 (C=O), 141.06

(A, C_4), 135.36 (A, C_2+C_6), 120.60 (A, C_3+C_5), 116.47 (A, C_1), 105.90 (CN), 31.54 (B, C_2), 29.10 (B, C_1). MS [m/z (% abundance)]: 101 (25), 118 (100), 198 (40), 298 (28). Elemental analysis calculated (%) for $C_{11}H_{10}N_2O_3Se_2 \cdot H_2O$: C: 41.92, H: 3.84, N: 8.89; found: C: 41.59, H: 3.58, N: 8.69.

*4.1.4.4. 3-[(4-Selenocyanatophenyl)carbamoyl]pyrazine-2-carboxylic acid (**4b**)*

From 2,3-pyrazinedicarboxylic anhydride. Conditions: 24 h at room temperature. The product was kept under stirring with water (25 mL) for 3 h, filtered, then stirred with ethyl ether (100 mL) for 24 h and then filtered. A yellow powder was obtained. Yield: 49.3%. Mp: 164–165ºC. IR (KBr) cm^{-1}: 3280 (NH), 2153 (CN), 1765 (C=O carboxylic acid), 1671 (C=O, amide). ^{1}H NMR (400 MHz, DMSO-d_6) δ: 13.82 (bs, 1H, COOH), 11.03 (s, 1H, NH), 8.92 (s, 2H, B, H_3+H_4), 7.87 (d, 2H, A, $J_{2\text{-}3}$=$J_{6\text{-}5}$= 8.6 Hz, H_2+H_6), 7.74 (d, 2H, A, $J_{3\text{-}2}$=$J_{5\text{-}6}$= 8.6 Hz, H_3+H_5). ^{13}C NMR (100 MHz, DMSO-d_6) δ: 167.05 (COOH), 163.64 (C=O), 146.99+146.75+146.15+145.49 (B, C_1+C_2+C_3+C_4), 140.49 (A, C_4), 135 (A, C_2+C_6), 122.19 (A, C_3+C_5), 118 (A, C_1), 106.37 (CN). MS [*m/z* (% abundance)]: 79 (100), 107 (95), 118 (30), 304 (75). Elemental analysis calculated (%) for $C_{13}H_8N_4O_3Se$: C: 44.97, H: 2.32, N: 16.14; found: C: 44.73, H: 2.72, N: 15.82.

*4.1.4.5. {2-Oxo-2-[(4-selenocyanatophenyl)amino]ethoxy}acetic acid (**5b**)*

From diglycolic anhydride. Conditions: 24 h at room temperature. The product was kept under stirring with water (25 mL) for 1 h, filtered and then washed with ethyl ether (2 × 25 mL). A white powder was obtained. Yield: 51.1%. Mp: 141–142ºC. IR (KBr) cm^{-1}: 3305 (NH), 2151 (CN), 1716 (C=O carboxylic acid), 1660 (C=O, amide). ^{1}H NMR (400 MHz, DMSO-d_6) δ: 12.91 (bs, 1H, COOH), 10.14 (s, 1H, NH), 7.74 (d, 2H, A, $J_{2\text{-}3}$=$J_{6\text{-}5}$= 8.8 Hz, H_2+H_6), 7.68 (d, 2H, A, $J_{3\text{-}2}$=$J_{5\text{-}6}$= 8.8 Hz, H_3+H_5), 4.21 (s, 2H, B, H_1), 4.20

(s, 2H, B, H_2). ^{13}C NMR (100 MHz, DMSO-d_6) δ: 172.25 (COOH), 168.78 (C=O), 140.14 (A, C_4), 135.27 (A, C_2+C_6), 121.30 (A, C_3+C_5), 117.43 (A, C_1), 105.92 (CN), 70.83 (B, C_1), 68.51 (B, C_2). MS [*m/z* (% abundance)]: 118 (85), 198 (40), 211 (30), 314 (100). Elemental analysis calculated (%) for $C_{11}H_{10}N_2O_4Se$: C: 42.19, H: 3.22, N: 8.95; found: C: 41.92, H: 3.53, N: 8.82.

*4.1.4.6. 2'-[(4-Selenocyanatophenyl)carbamoyl]-[1,1'-biphenyl]-2-carboxylic acid (**6b**)*

From diphenic anhydride. Conditions: 48 h at room temperature. The product was kept under stirring with water (25 mL) for 3 h, filtered and then washed with ethyl ether (2 × 25 mL). A white powder was obtained. Yield: 21.8%. Mp: 146–147ºC. IR (KBr) cm^{-1}: 3296 (NH), 2153 (CN), 1726 (C=O, carboxylic acid), 1631 (C=O, amide). ^{1}H NMR (400 MHz, DMSO-d_6) δ: 12.80 (bs, 1H, COOH), 10.24 (s, 1H, NH), 7.83 (d, 1H, B, $J_{9\text{-}10}$=7.6 Hz, H_9), 7.67–7.58 (m, 3H, B, H_2+H_5+H_{12}), 7.58–7.48 (m, 5H, A, H_2+H_3+H_5+H_6, B, H_{11}),7.41 (t, 1H, B, $J_{4\text{-}3}$=$J_{4\text{-}5}$= 7.4 Hz, H_4), 7.24 (t, 2H, B, $J_{3\text{-}2}$=$J_{3\text{-}4}$=$J_{10\text{-}9}$=$J_{10\text{-}11}$= 5.9 Hz, H_3+H_{10}). ^{13}C NMR (100 MHz, DMSO-d_6) δ: 169.20 (COOH), 167.55 (C=O), 141.41 (A, C_4), 140.79+140.76 (B, C_6+C_7), 136.14 (B, C_8), 135.19 (A, C_2+C_6), 131.67 (B, C_1), 131.42+131.07+130.45+130.11+129.84 (B, C_2+C_3+C_4+C_9+C_{11}), 127.88+127.78+127.55 (B, C_5+C_{10}+C_{12}), 121.06 (A, C_3+C_5), 117.14 (A, C_1), 105.89 (CN). MS [*m/z* (% abundance)]: 152 (70), 181 (100), 225 (30), 422 (10). Elemental analysis calculated (%) for $C_{21}H_{14}N_2O_3Se \cdot 2H_2O$: C: 55.15, H: 3.97, N: 6.13; found: C: 55.39, H: 3.59, N: 6.22.

*4.1.4.7. 2-[(4-Selenocyanatophenyl)carbamoyl]cyclohexanecarboxylic acid (**7b**)*

From cis-1,2-cyclohexanecarboxylic anhydride. Conditions: 24 h at room temperature. The product was kept under stirring with water (25 mL) for 2 h, filtered and then

washed with ethyl ether (2 × 25 mL). A white powder was obtained. Yield: 47.0%. Mp: 150–151ºC. IR (KBr) cm^{-1}: 3335 (NH), 2152 (CN), 1702 (C=O, carboxilic acid), 1677 (C=O, amide) ^{1}H NMR (400 MHz, DMSO-d_6) δ: 11.99 (bs, 1H, COOH), 9.95 (s, 1H, NH), 7.66 (d, 2H, A, $J_{2\text{-}3}$=$J_{6\text{-}5}$= 8.5 Hz, H_2+H_6), 7.62 (d, 2H, A, $J_{3\text{-}2}$=$J_{5\text{-}6}$= 8.5 Hz, H_3+H_5), 2.94 (d, 1H, B, $J_{1\text{-Hchex}}$= 4.0 Hz, H_1), 2.60 (d, 1H, B, $J_{\text{chex-1}}$ = 4.0 Hz, H_{chex}), 2.09 (d, 1H, B, J= 9.7 Hz, H_{chex}), 1.99 (d, 1H, B, J= 8.8 Hz, H_{chex}), 1.82–1.57 (m, 3H, B, 3Hchex), 1.48–1.24 (m, 3H, B, 3Hchex). ^{13}C NMR (100 MHz, DMSO-d_6) δ: 175.55 (COOH), 173.56 (C=O), 141.39 (A, C_4), 135.24 (A, C_2+C_6), 120.76 (A, C_3+C_5), 116.18 (A, C_1), 105.87 (CN), 43.05+42.42 (B, C_1+C_2), 28.06+25.64+24.44+22.78 (B, C_3+C_4+C_5+C_6). MS [*m/z* (% abundance)]: 67 (90), 81 (93), 118 (100), 198 (60), 334 (100). Elemental analysis calculated (%) for $C_{15}H_{16}N_2O_3Se \cdot H_2O$: C: 48.79, H: 4.91, N: 7.59; found: C: 48.56, H: 4.72, N: 7.66.

*4.1.4.8. 3-[(4-Selenocyanatophenyl)carbamoyl]-7-oxabicyclo[2.2.1]hept-5-ene-2-carboxylic acid (**8b**)*

From 3,6-epoxy-1,2,3,6-tetrahydrophthalic anhydride obtained by the classic procedure described for a Diels-Alder reaction using furan and maleic anhydride as reagents to yield the Diels-Alder adduct. Conditions: 24 h at room temperature. The product was kept under stirring with water (25 mL) for 4 h, filtered and then washed with ethyl ether (2 × 25 mL). A light-yellow powder was obtained. Yield: 20.3%. Mp: 155–156ºC. IR (KBr) cm^{-1}: 3267 (NH), 1711 (C=O carboxylic acid), 1689 (C=O, amide). ^{1}H NMR (400 MHz, DMSO-d_6) δ: 12.19 (s, 1H, COOH), 10.03 (s, 1H, NH), 7.65 (d, 2H, A, $J_{2\text{-}3}$=$J_{6\text{-}5}$= 9.0 Hz, H_2+H_6), 7.62 (d, 2H, A, $J_{3\text{-}2}$=$J_{5\text{-}6}$= 9.0 Hz, H_3+H_5), 6.50 (s, 2H, B, H_3+H_5), 5.14 (s, 1H, B, H_5), 5.06 (s, 1H, B, H_2), 2.82 (d, 1H, B, $J_{1\text{-}6}$= 9.1 Hz, H_1), 2.71 (d, 1H, B, $J_{6\text{-}1}$= 9.1 Hz, H_6). ^{13}C NMR (100 MHz, DMSO-d_6) δ: 173.08 (COOH),

170.48 (C=O), 141.07 (A, C_4), 137.49+137.08 (B, C_4+C_5), 135.29 (A, C_2+C_6), 120.79 (A, C_3+C_5), 116.51 (A, C_1), 105.93 (CN), 80.82+79.61 (B, C_3+C_6), 47.96+47.36 (B, C_1+C_2). ^{77}Se NMR (76 MHz, DMSO-d_6) δ: 320.95 (SeCN). MS [*m/z* (% abundance)]: 68 (100), 118 (100), 198 (25), 278 (10). Elemental analysis calculated (%) for $C_{15}H_{12}N_2O_4Se \cdot ½\ H_2O$: C: 48.35, H: 3.49, N: 7.52; found: C: 48.30, H: 3.70, N: 7.53.

4.2. Biological evaluation

4.2.1. Cell cultures

Cell lines were purchased from the American Type Culture Collection (ATCC). PC-3, HTB-54, HT-29, MOLT-4, CCRF-CEM, K-562 and MCF-7 cell lines were grown in RPMI 1640 medium (Gibco) supplemented with 10% fetal bovine serum (FBS; Gibco), 100 units/mL penicillin and 100 mg/mL streptomycin (Gibco). BEAS-2B cell line (normal epithelial lung) was cultured in DMEM (Gibco), 10% FBS, 100 units/mL penicillin and 100 μg/mL streptomycin. 184B5 cells were grown in DMEM/F12 medium supplemented with 5% FBS, 1× ITS (Lonza), 100 nM hydrocortisone (Aldich), 2 mM sodium pyruvate (Lonza), 20 ng/mL EGF (Sigma- Aldrich), 0.3 nM *trans*-retinoic acid (Sigma-Aldrich), 100 units/mL penicillin and 100 mg/mL streptomycin. Cells were maintained at 37ºC and 5% CO_2.

4.2.2. Cytotoxic and antiproliferative activities

Cell viability was determined using the MTT 3-(4,5-dimethylthiazol-2-yl)-2,5-diphenyl-tetrazolium bromide) method at 10 and 100 μM to perform the screening. In order to build full dose-response curves five different doses ranging from 0.01 to 100 μM, for some compounds lower doses where needed in order to reach 50% cell growth. Depending on cell size, 8,000 to 40,000 cells were seeded per well in 96-well plates and incubated overnight. Then treated with the compounds for 48 h, cells were then

incubated with 50 μL of MTT (2 mg/mL stock) for 4 h, medium was removed by aspiration and formazan crystals dissolved in 150 μL of DMSO. The absorbance was measured at 550 nm in a microplate reader (Sunrise reader, Tecan). At least three independent experiments performed in quadruplicate were analysed. Results are expressed as GI_{50}, the concentration that reduces by 50% the growth of treated cells with respect to untreated controls, TGI, the concentration that completely inhibits cell growth, and LC_{50}, the concentration that kills 50% of the cells.

4.2.3. Evaluation of cell cycle progression and cell death

A fixed population of MCF-7 cells per flask were seeded in 25 cm^2 flasks then incubated overnight. Cultures were treated with the corresponding amount of compounds **10a**, **8b**, DMSO (control) or 6 μM camptothecin (positive control). Seeded population was dependent on studied time point: 3×10^6 cells/flask for 24 h or shorter treatment, 2×10^6 cells/flasks for 48 h treatment and finally 1×10^6 cells/flask for 72 h experiments. Apo-Direct kit (BD Pharmigen) was used to determine cell cycle distribution and cell death percentage. Cells were fixed in a 1% paraformaldehyde solution in PBS for 30–40 min at 0ºC, washed with PBS twice and incubated for 30 min with 70% ethanol on ice. Staining was performed following manufacturer's protocol and samples were analysed by flow cytometry using a Counter Epics XL cytometer (Beckman Counter).

Inhibition assays cells were pre-treated with 50 μM of the pan-caspase inhibitor Z-VAD-FMK (BD Pharmigen) or 100 nM of the autophagy inhibitor wortmannin (Santa Cruz) for 1 h or 10 μM of chloroquine (Sigma Aldrich). The cells were treated with 80 μM of **8b** or **10a**, DMSO was added to the control cells. Samples were processed

following the same methodology stated above. At least three independent experiments were performed in duplicate.

4.2.4. Statistical analysis

Statistical data represent the mean ± SEM of at least three independent experiments performed in duplicate. Mann-Whitney U-test was used to stablish statistical significance of differences between control and treatment groups. GraphPad Prism version 7 was used, significant differences were considered at $p < 0.05$.

4.2.5. Protein analysis

Proteins were detected by western blot. Specific antibodies for LC3B, Beclin-1 (D40C5), SQSTM1/p62, AMPK, JNK, pAKT (Se473) and the PI3K catalytic subunit p110α were obtained from Cell Signalling. Anti-actin (H-300) was from Santa Cruz Biotechnology. Anti-rabbit IgG conjugated with peroxidase (Cell Signaling) was used as secondary antibody.

Acknowledgments

The research leading to these results has received funding from "la Caixa" Banking Foundation. P. Garnica wishes to express his gratitude to the Asociación de Amigos de la Universidad de Navarra for the pre-doctoral fellowship. Furthermore, the authors wish to express their gratitude to the Plan de Investigación de la Universidad de Navarra, PIUNA (Ref 2014–26) as well as Caixa Foundation-UNED for financial support for the project.

References

[1] R.L. Siegel, K.D. Miller, A.A.-O.h.o.o. Jemal, Cancer statistics, 2018, Ca-Cancer J. Clin. 68 (2018) 7-30. https://doi.org/10.3322/caac.21442.

[2] P. Bhat, J. Kriel, B. Shubha Priya, Basappa, N.S. Shivananju, B. Loos, Modulating autophagy in cancer therapy: Advancements and challenges for cancer cell death sensitization, Biochem. Pharmacol. 147 (2018) 170-182. https://doi.org/10.1016/j.bcp.2017.11.021.

[3] C. Bi, N. Zhang, P. Yang, C. Ye, Y. Wang, T. Fan, R. Shao, H. Deng, D. Song, Synthesis, biological evaluation, and autophagy mechanism of 12N-substituted sophoridinamines as novel anticancer agents, ACS Med. Chem. Lett. 8 (2017) 245-250. https://doi.org/10.1021/acsmedchemlett.6b00466.

[4] Y.Y. Zhou, Y. Li, W.Q. Jiang, L.F. Zhou, MAPK/JNK signalling: A potential autophagy regulation pathway, Biosci. Rep. 35 (2015). https://doi.org/10.1042/BSR20140141.

[5] D.D. Li, L.L. Wang, R. Deng, J. Tang, Y. Shen, J.F. Guo, Y. Wang, L.P. Xia, et al., The pivotal role of c-JUN NH2-terminal kinase-mediated Beclin 1 expression during anticancer agents-induced autophagy in cancer cells, Oncogene 28 (2009) 886-898. https://doi.org/10.1038/onc.2008.441.

[6] R.C. Russell, H.X. Yuan, K.L. Guan, Autophagy regulation by nutrient signaling, Cell Res. 24 (2014) 42-57. https://doi.org/10.1038/cr.2013.166.

[7] K. Inoki, T. Zhu, K.L. Guan, TSC2 mediates cellular energy response to control cell growth and survival, Cell 115 (2003) 577-590. https://doi.org/https://doi.org/10.1016/S0092-8674(03)00929-2.

[8] S. Kanno, S. Yomogida, A. Tomizawa, H. Yamazaki, K. Ukai, R.E.P. Mangindaan, M. Namikoshi, M. Ishikawa, Papuamine causes autophagy following the reduction of

cell survival through mitochondrial damage and JNK activation in MCF-7 human breast cancer cells, Int. J. Oncol. 43 (2013) 1413-1419. https://doi.org/10.3892/ijo.2013.2093.

[9] Z.L. Sun, J.L. Dong, J. Wu, Juglanin induces apoptosis and autophagy in human breast cancer progression via ROS/JNK promotion, Biomed. Pharmacother. 85 (2017) 303-312. https://doi.org/10.1016/j.biopha.2016.11.030.

[10] S. Kang, J.E. Kim, N.R. Song, S.K. Jung, M.H. Lee, J.S. Park, M.H. Yeom, A.M. Bode, Z. Dong, K.W. Lee, The ginsenoside 20-o-beta-d-glucopyranosyl-20(S)-protopanaxadiol induces autophagy and apoptosis in human melanoma via AMPK/JNK phosphorylation, PLoS One 9 (2014) e104305. https://doi.org/10.1371/journal.pone.0104305.

[11] A. Puissant, G. Robert, N. Fenouille, F. Luciano, J.P. Cassuto, S. Raynaud, P. Auberger, Resveratrol promotes autophagic cell death in chronic myelogenous leukemia cells via JNK-mediated p62/SQSTM1 expression and ampk activation, Cancer Res. 70 (2010) 1042-1052. https://doi.org/10.1158/0008-5472.CAN-09-3537.

[12] Q. Miao, J. Xu, A. Lin, X. Wu, L. Wu, W. Xie, Recent advances for the synthesis of selenium-containing small molecules as potent antitumor agents, Curr. Med. Chem. 25 (2017) 2009-2033. https://doi.org/10.2174/0929867325666171129220544.

[13] D. Bartolini, L. Sancineto, A. Fabro de Bem, K.D. Tew, C. Santi, R. Radi, P. Toquato, F. Galli, Selenocompounds in cancer therapy: An overview, Adv. Cancer. Res. 136 (2017) 259-302. https://doi.org/10.1016/bs.acr.2017.07.007.

[14] Y. Yang, H. Luo, K. Hui, Y. Ci, K. Shi, G. Chen, L. Shi, C. Xu, Selenite-induced autophagy antagonizes apoptosis in colorectal cancer cells *in vitro* and *in vivo*, Oncol. Rep. 35 (2016) 1255-1264. https://doi.org/10.3892/or.2015.4484.

[15] J.C. Wu, F.Z. Wang, M.L. Tsai, C.Y. Lo, V. Badmaev, C.T. Ho, Y.J. Wang, M.H. Pan, Se-allylselenocysteine induces autophagy by modulating the AMPK/mTOR

signaling pathway and epigenetic regulation of PCDH17 in human colorectal adenocarcinoma cells, Mol. Nutr. Food.Res. 59 (2015) 2511-2522. https://doi.org/10.1002/mnfr.201500373.

[16] Y.F. Zou, P.Y. Niu, J. Yang, J. Yuan, T.C. Wu, X.M. Chen, The JNK signaling pathway is involved in sodium-selenite-induced apoptosis mediated by reactive oxygen in HEPG2 cells, Cancer Biol. Ther. 7 (2008) 689-696. https://doi.org/10.4161/cbt.7.5.5688.

[17] K. Wang, X.T. Fu, Y. Li, Y.J. Hou, M.F. Yang, J.Y. Sun, S.Y. Yi, C.D. Fan, et al., Induction of S-phase arrest in human glioma cells by selenocysteine, a natural selenium-containing agent via triggering reactive oxygen species-mediated DNA damage and modulating MAPKs and AKT pathways, Neurochem. Res. 41 (2016) 1439-1447. https://doi.org/10.1007/s11064-016-1854-8.

[18] P. Chakraborty, S.S. Roy, A. Basu, S. Bhattacharya, Sensitization of cancer cells to cyclophosphamide therapy by an organoselenium compound through ROS-mediated apoptosis, Biomed. Pharmacother. 84 (2016) 1992-1999. https://doi.org/10.1016/j.biopha.2016.11.006.

[19] C. Kim, J. Lee, M.-S. Park, Synthesis of new diorganodiselenides from organic halides: Their antiproliferative effects against human breast cancer MCF-7 cells, Arch. Pharm. Res. 38 (2014) 659-665. https://doi.org/10.1007/s12272-014-0407-4.

[20] D. Plano, Y. Baquedano, E. Ibanez, I. Jimenez, J.A. Palop, J.E. Spallholz, C. Sanmartin, Antioxidant-prooxidant properties of a new organoselenium compound library, Molecules 15 (2010) 7292-7312. https://doi.org/10.3390/molecules15107292.

[21] P. Garnica, I. Encio, D. Plano, J.A. Palop, C. Sanmartin, Combined acylselenourea-diselenide structures: New potent and selective antitumoral agents as

autophagy activators, ACS Med. Chem. Lett. 9 (2018) 306-311. https://doi.org/10.1021/acsmedchemlett.7b00482.

[22] V. Bala, S. Rao, P. Li, S. Wang, C.A. Prestidge, Lipophilic prodrugs of SN38: Synthesis and in vitro characterization toward oral chemotherapy, Mol. Pharm. 13 (2015) 287-294. https://doi.org/10.1021/acs.molpharmaceut.5b00785.

[23] M. Majekova, J. Ballekova, M. Prnova, M. Stefek, Structure optimization of tetrahydropyridoindole-based aldose reductase inhibitors improved their efficacy and selectivity, Bioorg. Med. Chem. 25 (2017) 6353-6360. https://doi.org/10.1016/j.bmc.2017.10.005.

[24] G. Huang, A. Drakopoulos, M. Saedtler, H. Zou, L. Meinel, J. Heilmann, M. Decker, Cytotoxic properties of the alkaloid rutaecarpine and its oligocyclic derivatives and chemical modifications to enhance water-solubility, Bioorg. Med. Chem. Lett. 27 (2017) 4937-4941. https://doi.org/10.1016/j.bmcl.2017.08.045.

[25] V. Gota, J.S. Goda, K. Doshi, A. Patil, S. Sunderajan, K. Kumar, M. Varne, A. Kunwar, V.K. Jain, I. Priyadarshini, Biodistribution and pharmacokinetic study of 3,3′ diseleno dipropionic acid (DSEPA), a synthetic radioprotector, in mice, Eur. J. Drug Metabol. 41 (2015) 839-844. https://doi.org/10.1007/s13318-015-0301-6.

[26] K.E. Machado, K.N. Oliveira, L. Santos-Bubniak, M.A. Licinio, R.J. Nunes, M.C. Santos-Silva, Evaluation of apoptotic effect of cyclic imide derivatives on murine B16F10 melanoma cells, Bioorg. Med. Chem. 19 (2011) 6285-6291. https://doi.org/10.1016/j.bmc.2011.09.008.

[27] D. Rosolen, I.F. Kretzer, E. Winter, V.F. Noldin, I.A. Rodrigues do Carmo, F.B. Filippin-Monteiro, V. Cechinel-Filho, T.B. Creczynski-Pasa, N-phenylmaleimides affect adipogenesis and present antitumor activity through reduction of FASN

expression, Chem. Biol. Interact. 258 (2016) 10-20. https://doi.org/10.1016/j.cbi.2016.08.005.

[28] B. Romano, D. Plano, I. Encio, J.A. Palop, C. Sanmartin, In vitro radical scavenging and cytotoxic activities of novel hybrid selenocarbamates, Bioorg. Med. Chem. 23 (2015) 1716-1727. https://doi.org/10.1016/j.bmc.2015.02.048.

[29] E. Dominguez-Alvarez, D. Plano, M. Font, A. Calvo, C. Prior, C. Jacob, J.A. Palop, C. Sanmartin, Synthesis and antiproliferative activity of novel selenoester derivatives, Eur. J. Med. Chem. 73 (2014) 153-166. https://doi.org/10.1016/j.ejmech.2013.11.034.

[30] V. Alcolea, D. Plano, D.N. Karelia, J.A. Palop, S. Amin, C. Sanmartin, A.K. Sharma, Novel seleno- and thio-urea derivatives with potent in vitro activities against several cancer cell lines, Eur. J. Med. Chem. 113 (2016) 134-144. https://doi.org/10.1016/j.ejmech.2016.02.042.

[31] V. Alcolea, D. Plano, I. Encio, J.A. Palop, A.K. Sharma, C. Sanmartin, Chalcogen containing heterocyclic scaffolds: New hybrids with antitumoral activity, Eur. J. Med. Chem. 123 (2016) 407-418. https://doi.org/10.1016/j.ejmech.2016.07.042.

[32] N. Diaz-Argelich, I. Encio, D. Plano, A.P. Fernandes, J.A. Palop, C. Sanmartin, Novel methylselenoesters as antiproliferative agents, Molecules 22 (2017) 1288. https://doi.org/10.3390/molecules22081288.

[33] M. Diaz, R. Gonzalez, D. Plano, J.A. Palop, C. Sanmartin, I. Encio, A diphenyldiselenide derivative induces autophagy via JNK in HTB-54 lung cancer cells, J. Cell. Mol. Med. 22 (2018) 289-301. https://doi.org/10.1111/jcmm.13318.

[34] Z. Han, B. Li, J. Wang, X. Zhang, Z. Li, L. Dai, M. Cao, J. Jiang, Norcantharidin inhibits SK-N-SH neuroblastoma cell growth by induction of autophagy and apoptosis,

Technol. Cancer Res. Treat. 16 (2016) 33-44. https://doi.org/10.1177/1533034615624583.

[35] M. Dalvai, K. Bystricky, Cell cycle and anti-estrogen effects synergize to regulate cell proliferation and ER target gene expression, PLoS One 5 (2010) e11011. https://doi.org/10.1371/journal.pone.0011011.

[36] H. Hamouchene, V.M. Arlt, I. Giddings, D.H. Phillips, Influence of cell cycle on responses of MCF-7 cells to benzo[a]pyrene, BMC Genomics 12 (2011) 333. https://doi.org/10.1186/1471-2164-12-333.

[37] M. Hamada, H. Kameyama, S. Iwai, Y. Yura, Induction of autophagy by sphingosine kinase 1 inhibitor PF-543 in head and neck squamous cell carcinoma cells, Cell Death Discov. 3 (2017) 17047. https://doi.org/10.1038/cddiscovery.2017.47.

[38] P. Fabbrizio, S. Amadio, S. Apolloni, C. Volonte, P2x7 receptor activation modulates autophagy in SOD1-G93A mouse microglia, Front. Cell. Neurosci. 11 (2017) 249. https://doi.org/10.3389/fncel.2017.00249.

[39] H.J. Jung, J.H. Kang, S. Choi, Y.K. Son, K.R. Lee, J.K. Seong, S.Y. Kim, S.H. Oh, Pharbitis nil (PN) induces apoptosis and autophagy in lung cancer cells and autophagy inhibition enhances PN-induced apoptosis, J. Ethnopharmacol. 208 (2017) 253-263. https://doi.org/10.1016/j.jep.2017.07.020.

[40] D.J. Klionsky, K. Abdelmohsen, A. Abe, M.J. Abedin, H. Abeliovich, A. Acevedo Arozena, H. Adachi, C.M. Adams, et al., Guidelines for the use and interpretation of assays for monitoring autophagy (3rd edition), Autophagy 12 (2016) 1-222. https://doi.org/10.1080/15548627.2015.1100356.

[41] K. Wang, C. Zhang, J. Bao, X. Jia, Y. Liang, X. Wang, M. Chen, H. Su, et al., Synergistic chemopreventive effects of curcumin and berberine on human breast cancer

cells through induction of apoptosis and autophagic cell death, Sci. Rep. 6 (2016) 26064. https://doi.org/10.1038/srep26064.

[42] S. Faes, O. Dormond, PI3K and AKT: Unfaithful partners in cancer, Int. J. Mol. Sci. 16 (2015) 21138-21152. https://doi.org/10.3390/ijms160921138.

[43] X. Wu, S. Renuse, N.A. Sahasrabuddhe, M.S. Zahari, R. Chaerkady, M.S. Kim, R.S. Nirujogi, M. Mohseni, et al., Activation of diverse signalling pathways by oncogenic PIK3CA mutations, Nat. Commun. 5 (2014) 4961. https://doi.org/10.1038/ncomms5961.

[44] A. Guerrero-Zotano, I.A. Mayer, C.L. Arteaga, PI3K/AKT/mTOR: Role in breast cancer progression, drug resistance, and treatment, Cancer Metastasis Rev. 35 (2016) 515-524. https://doi.org/10.1007/s10555-016-9637-x.

[45] X.L. Xu, J. Sun, R.L. Song, M.E. Doscas, A.J. Williamson, J.S. Zhou, J. Sun, X.N. Jiao, X.F. Liu, Y. Li, Inhibition of p70 S6 kinase (S6K1) activity by A77 1726, the active metabolite of leflunomide, induces autophagy through TAK1-mediated AMPK and JNK activation, Oncotarget 8 (2017) 30438-30454. https://doi.org/10.18632/oncotarget.16737.

[46] J.N. Hutchinson, J. Jin, R.D. Cardiff, J.R. Woodgett, W.J. Muller, Activation of AKT-1 (PKB-alpha) can accelerate ERBB-2-mediated mammary tumorigenesis but suppresses tumor invasion, Cancer Res. 64 (2004) 3171-3178. https://doi.org/10.1158/0008-5472.

[47] S. Brolih, S.K. Parks, V. Vial, J. Durivault, L. Mostosi, J. Pouyssegur, G. Pages, V. Picco, AKT1 restricts the invasive capacity of head and neck carcinoma cells harboring a constitutively active PI3 kinase activity, BMC Cancer 18 (2018) 249. https://doi.org/10.1186/s12885-018-4169-0.